Exploiting the internal resonance in shunted circuit-based vibration suppression

EXPLOITING THE INTERNAL RESONANCE IN SHUNTED CIRCUIT-BASED VIBRATION SUPPRESSION

by

Khaled Al-Souqi

A Thesis presented to the Faculty of the
American University of Sharjah
College of Engineering
In Partial Fulfilment
of the Requirements
for the Degree of

Master of Science in
Mechanical Engineering

Sharjah, United Arab Emirates

Sep 2024

Declaration of Authorship

I declare that this project/thesis/dissertation is my own work and, to the best of my knowledge and belief, it does not contain material published or written by a third party, except where permission has been obtained and/or appropriately cited through full and accurate referencing.

Signed……………………Khaled Al-Souqi…………………………….

Date……………………30/09/2024……………………………

Approvals

We, the undersigned, approve the Master's Thesis written by: Khaled Al-Souqi

Thesis Title:

Exploiting the internal resonance in shunted circuit-based vibration suppression

Date of Defense: 30/09/2024

Name, Title and Affiliation	Signature
Dr. Samir Emam Professor Department of Mechanical Engineering Thesis Advisor	
Dr. Mohammad Jaradat Professor Department of Mechanical Engineering Thesis Examiner (Internal)	
Dr. Mohammad Al-Hamaydeh Professor Department of Civil Engineering Thesis Examiner (External)	

Accepted by:

Dr. Fadi Aloul
Dean
College/School of Engineering

Dr. Mohamed El-Tarhuni
Vice Provost for Research and Graduate Studies
Office of Research and Graduate Studies

Acknowledgments

First and foremost, I would like to express my deepest gratitude to my thesis advisor, Professor Samir Emam for his support and guidance throughout my master's journey. His dedication, patience, and constant monitoring have been invaluable to my development over the past two years. It has been an honor to work under his supervision, and I am truly grateful for the opportunity to learn from his expertise and both his academic and non-academic advices.

I would also like to thank Professor Samir Emam for introducing me to my research partner and brother, Khaled Kadri. Our collaboration pushed each other to grow and improve, and I am grateful for the shared journey, support, and motivation we gave one another along the way.

Also, I would like to thank my dear friend and brother Mohammed Elmahdi for his continuous support during my academic career since when we were undergrads, he played a huge role in encouraging me to pursue my graduate studies. Also, I would like to thank all my friends at AUS for the valuable memories that we shared.

Finally, I would like to thank the American University of Sharjah for supporting me in achieving my master's degree requirements under the Research Assistantship offered during my program.

Dedication

"To the hands that lifted me when I stumbled, the hearts that believed in me through doubt, and the unwavering love that carried me forward—this is for you, my family."

Abstract

Vibration reduction is an essential component of structural engineering that guarantees the functionality and endurance of numerous mechanical and architectural systems during design and maintenance. The field has been significantly improved in recent years with the introduction of piezoelectric materials, which provide novel solutions for regulating and mitigating vibrations. This thesis presents an approach to enhance vibration attenuation in cantilever structures by integrating piezoelectric patches and a shunt circuit, thereby advancing the field of vibration control in cantilever structures. The thesis begins with an introduction that provides a thorough overview of the classifications of vibration control and the importance attributed to vibration attenuation techniques. A comprehensive literature review aims to analyze previous studies and their methodologies in piezoelectric material vibration control is provided. A mathematical model that governs the dynamics of a cantilever beam combined with a piezoelectric transducer and a shunted circuit is developed. The model's initial emphasis is on the single-mode vibration occurring within a linear structure. The major innovation of this study is the systemic integration of a nonlinear electrical component that is introduced to activate the two-to-one internal resonance. The internal resonance is a nonlinear phenomenon that has demonstrated the potential to enhance the suppression of vibrations significantly. In order to attain optimal attenuation efficiency, the mathematical model is numerically simulated using MATLAB. This process includes modifying the shunt circuit's electrical parameters and tuning the absorber's frequencies with the structure’s natural frequency. Moreover, the model is extended to account for the nonlinearity of the host structure to examine the robustness of the proposed model. The main outcome of this study is a development in the domain of vibration control, providing a solution for engineering applications that require vibration attenuation that is both more effective and adaptable.

Keywords: Vibration Suppression; Internal Resonance; Piezoelectric Shunted Circuit; Nonlinear Dynamics.

Contents

List of Figures

List of Tables

Chapter 1. Introduction

In this chapter, we introduce vibration damping and how it can be conducted by a shunted circuit, exploring several types of control methodologies. We also discuss the contribution of internal resonances to vibration attenuation. Then, we present the thesis objectives and contribution. Finally, the thesis organization is outlined at the end of this chapter.

1.1. Overview

Mechanical vibration is essential to the study of dynamic systems and structural integrity. These vibrations can emerge in various ways ranging from minor oscillations to catastrophic movements. In many mechanical systems, vibration is undesirable and even harmful. For example, vibration in an airplane frame induces fatigue and can eventually lead to failure [1]. Therefore, it is essential to consider the consequences of vibration while constructing engineering machines and structures. As a result, efficiently dampening vibrations has become critical in a wide range of technical applications.

1.1.1. Background

It is essential to recognize the strategies that have been important in engineering and construction as we examine vibration-damping techniques. Traditional methods, such as mass-dampers and viscoelastic materials, have long been reliable instruments for reducing vibrations and providing effective solutions to practical problems. However, they often exhibit limitations in terms of adaptability, accuracy, and efficiency. Nonetheless, innovation always intends to push boundaries in the dynamic realm of vibration control. Piezoelectric shunted circuits are one such innovation that has drawn growing interest. In 1880, Pierre and Jacques Curie first discovered the piezoelectric effect. They showed that once certain crystalline materials were stressed, a counter-reaction happened. The piezoelectric effect has two types: the direct effect, which describes how a material can convert mechanical strain into electrical charge, and the reverse effect, which describes how a material can transform an applied electrical potential into mechanical strain energy [2]. In 1979, Forward [3] proposed changing the system's physical parameters to control the vibration of a structure by converting the dynamic strain energy from the structure into electrical energy using piezoelectric transducers connected to an electrical impedance, as demonstrated in Figure 1. From that day onwards, the development of Forward invention didn't stop.

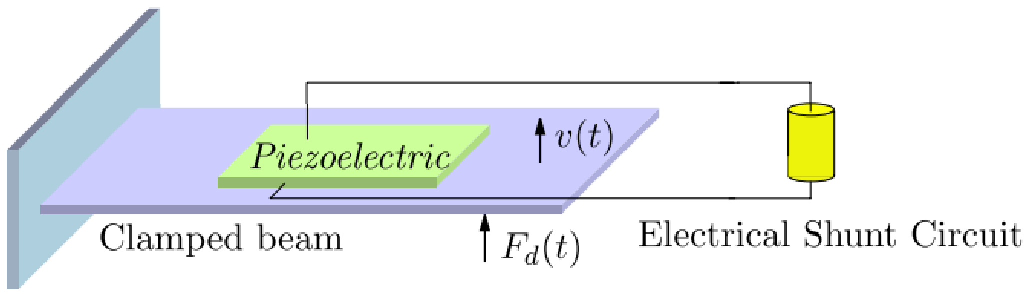

Figure 1: A cantilever beam coupled with an electrical shunted circuit by a piezoelectric patch [4].

1.1.2. Shunted Circuit Classifications

The researchers divided the types of piezoelectric shunted circuits into three subcategories based on their controlling techniques: passive, active, and semi-active. The choice of one of those types depends on the electrical elements in the shunted circuits and the presence of any external energy source. The passive technique relies on the inherent ability of piezoelectric material to absorb vibrational energy, resulting in passive energy dissipation without any external power source. On the other hand, active methods utilize sensors and actuators to achieve vibration sensing and activation to suppress vibration in real time [5]. The active control method has successfully reduced vibration in a wide range of structures, from simple beams to more complicated space structures. An active control system frequently requires powerful power amplifiers and high-performance digital signal processors, which are inappropriate for space applications, to drive actuators. Despite being simpler to construct than active control systems, passive control methods are less resistant to system disturbances [6]. Therefore, the interest in semi-active control systems has increased because of their potential to successfully offer vibration damping using piezoelectric materials. These systems combine the benefits of adaptability and energy efficiency to provide an adaptable way of reducing vibrations in various applications. It is essential to keep in mind that while active damping can be used to limit low-frequency vibrations, passive damping can be highly effective at damping high-frequency excitations. Additionally, Semi-active damping techniques are necessary for good control over wide frequency bands, where the semi-active method combines the best attributes from active and passive approaches [7].

1.1.3. Internal Resonances

Each vibration mode in a purely linear structure can be excited independently, for example, by applying an external force, leaving the other modes at rest; however, this isn't necessarily the case in nonlinear systems. Internal resonances take place when two modes of a nonlinear system are mutually synchronized [8], which means their frequencies are in a simple integer ratio. This condition can be utilized to result in a unique interaction between these modes, known as saturation phenomena. The saturation phenomenon was first discovered by Nayfeh et al. [9], which causes an energy exchange by creating a threshold for one of the modes and transferring the energy to the other mode whenever an external excitation is applied to the first mode. This technique can significantly influence the vibration amplitude and system behavior. The type of nonlinearity coupling between the modes and tuning the frequency ratio between them determines the type of internal resonance in the system. If the frequency ratio between the modes is doubled, then a quadratic nonlinearity in the system is required to achieve a 2:1 internal resonance. Also, another type of internal resonance, 3:1, is caused by cubic nonlinearity when the frequency ratio of the two modes equals three [10].

1.2. Thesis Objectives

Driven by the interest in exploring the physics behind vibration damping associated with nonlinearities in the system, we focus on developing a model that can exploit internal resonance to achieve a high damping performance. The model consists of a cantilever beam (structure), a piezoelectric patch (transducer), and the shunted circuit (nonlinear absorber), which will contain a nonlinear electrical component to create the internal resonance. Tuning in frequencies to achieve internal resonance and choosing the optimal circuit parameters will be conducted by performing a parametric study. Moreover, the absorber's performance dealing with other sources of nonlinearity, such as geometrical nonlinearity, will be analyzed and discussed.

1.3. Research Contribution

The contributions of this research work are summarized as follows:

- Developing a nonlinear vibration absorber that utilizes the internal resonance phenomena to dampen the vibration of a linear structure by tuning the electromechanical frequencies and optimizing circuit parameters.
- Investigating the performance of the nonlinear absorber when dealing with another source of nonlinearity from the structure for a single vibration mode.

1.4. Thesis Organization

The rest of the thesis is organized as follows:

Chapter 2 provides extensive literature on the work that has been done on vibration damping by shunted circuits and the previous utilization of internal resonance in that matter. Chapter 3 discusses a detailed formulation for the model and the implementation of nonlinear electrical components on the shunted circuit. It also introduces the implementation of nonlinearity into the structure. Chapter 4 presents the results obtained from numerically simulating the model in Chapter 3. Chapter 5 concludes the work and discusses future work, and finally, the reference list is presented.

Chapter 2. Literature Review

This chapter covers shunted circuit vibration control methods, including active, passive, and semi-active systems. The literature review aims to explore more about these systems' capabilities, drawbacks, and how internal resonance might improve vibration control. This review attempts to provide a comprehensive picture of the status of shunted circuit technology in vibration control and what has been done until now.

2.1. Passive Vibration Control

In some applications, the passive vibration-dampening techniques using piezoelectric transducers have significant advantages. For example, its ability to operate without active control systems or external power simplifies implementation and minimizes energy consumption. Those advantages significantly brought it to light and made it preferable over other control methods. Hagood and Flotow [11] were the first to investigate the idea of using a piezoelectric transducer connected to a passive electrical circuit to dissipate mechanical energy. They achieved this by connecting the piezoelectric transducer to a resistor, as shown in Figure 2a, which acts as a viscoelastic damper. Moreover, they added a series resistor-inductor circuit (resonant) to the system in a different instance as illustrated in Figure 2b. To mitigate the maximum vibration amplitude by the RL circuit, they adjusted the electric circuit's impedance frequency to match the structural resonance frequency for a single mode. Their method has a drawback: large inductors are needed to achieve the low electrical resonance needed to dampen a low-frequency resonance.

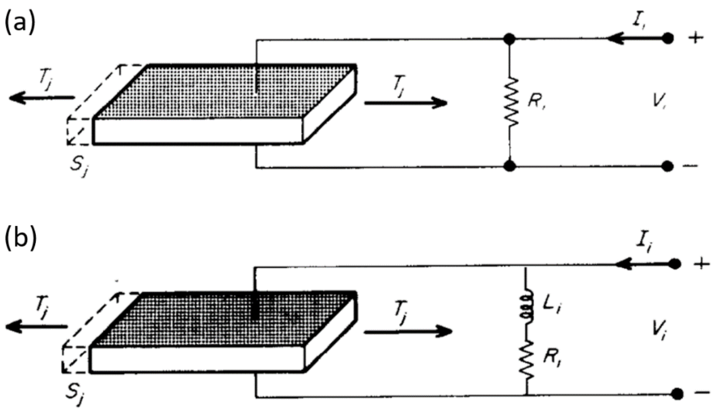

Figure 2: a) Piezoelectric patch coupled to a resistor. b) Piezoelectric patch coupled to an RL circuit [11].

Many researchers tried to solve the drawbacks that Hagood and Flotow [11] faced in their work [12]. Yamada [13] proposed using a multi-layered piezoelectric transducer connected to a (RL) circuit. The purpose of multi-layering the piezoelectric element was to increase its capacitance, reducing the requirement for a high inductance value at low frequencies. Figure 3 shows the model that was used to illustrate the effect of a multi-layered piezoelectric patch. The author ignored using a resistive shunt circuit because of their low damping contribution. Another approach to solving this problem was proposed by Lossouarn et al. [14]. The research investigates how to improve inductance values using closed magnetic cores composed of materials with high permeability. It demonstrates how customized designs can enable the use of passive resonant shunt techniques at lower frequencies.

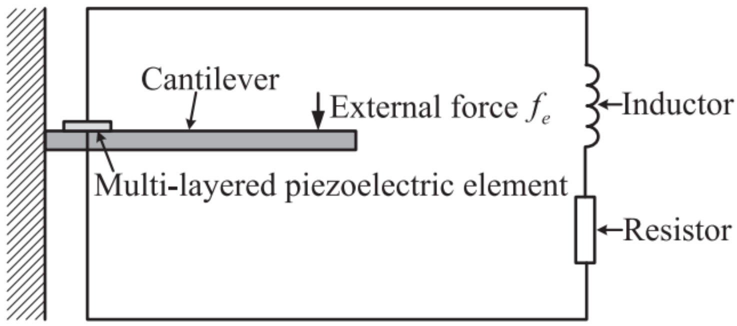

Figure 3: A model for a multi-layered piezoelectric patch on a cantilever beam with RL circuit [13].

Previous works have focused on utilizing a single piezoelectric device to suppress a single structural mode. However, many systems have several vibration modes, which have a massive role in the system's vibration. Holkamp [15] was able to develop an approach for suppressing multiple modes using a single piezoelectric element. Additional L-R-C circuit branches are coupled parallel to an RL branch into a single piezoelectric component, as demonstrated in Figure 4. The number of RLC branches equals the number of modes chosen to be damped. A cantilevered beam was used to test the multimode damper experimentally. In the second and third bending modes, the results showed reductions in vibration amplitude of 19 dB and 12 dB, respectively. Holkamp's work was lacking in presenting a control method to tune each branch separately.

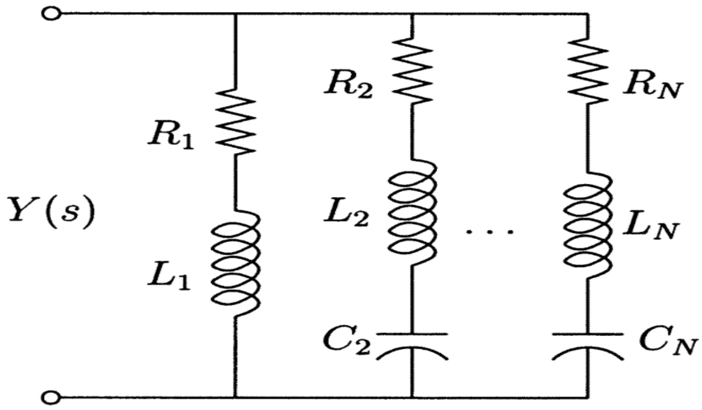

Figure 4: Holkamp circuit [15].

Many researchers have proposed other circuit configurations to control the branches. Wu [16,17] have developed a multi-mode shunt that utilizes a current-blocking circuit, as shown in Figure 5a. The electrical impedance of the LC anti-resonant circuits is designed to reach infinity and act as an open circuit at other branch frequencies, while the targeted branch that matches the resonance frequency of the structure operates and damps the vibration. On the other hand, Behrens et al. [18,19] It is proposed using “current-flowing” branches in the shunted circuit, as demonstrated in Figure 5b. The function of the current-blocking shunt and the current-flowing shunt is similar. The current-flowing shunt permits the current to flow rather than stopping it at the natural frequency. This method is better than "current-blocking" because the latter requires an equal number of inductors for each mode.

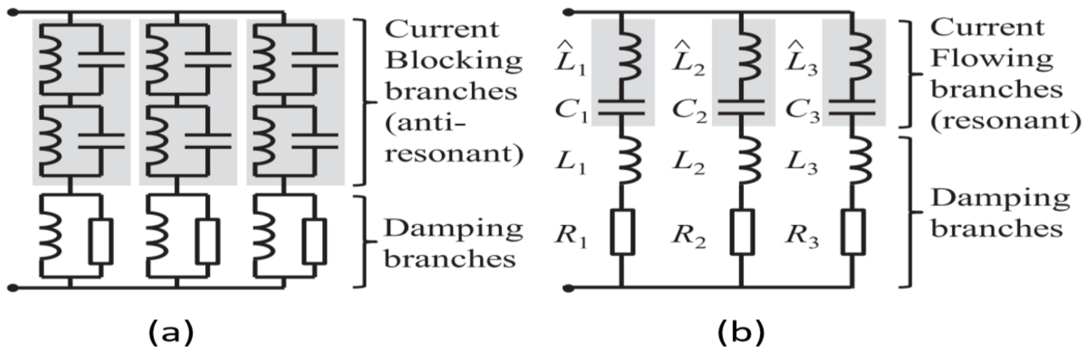

Figure 5: a) Current Blocking circuit. b) Current Flowing circuit [20].

Raze et al. [21] introduced a groundbreaking tuning approach for a simplified current-blocking shunt circuit, a method they validated using a cantilever beam both numerically and experimentally. Their innovative strategy, which focuses on the impact of non-resonant modes and the electromechanical coupling between the structure and the shunt branches, aims to improve multimode damping without the need for any optimization algorithm. The approach's ability to control many modes is demonstrated through the frequency response (FRF) for the first four modes, as shown in Figure 6. This approach stands out from others that use optimization algorithms for tuning circuit parameters, such as Particle swarm optimization [22,23], Ant colony optimization [24], and other tuning techniques [25,26].

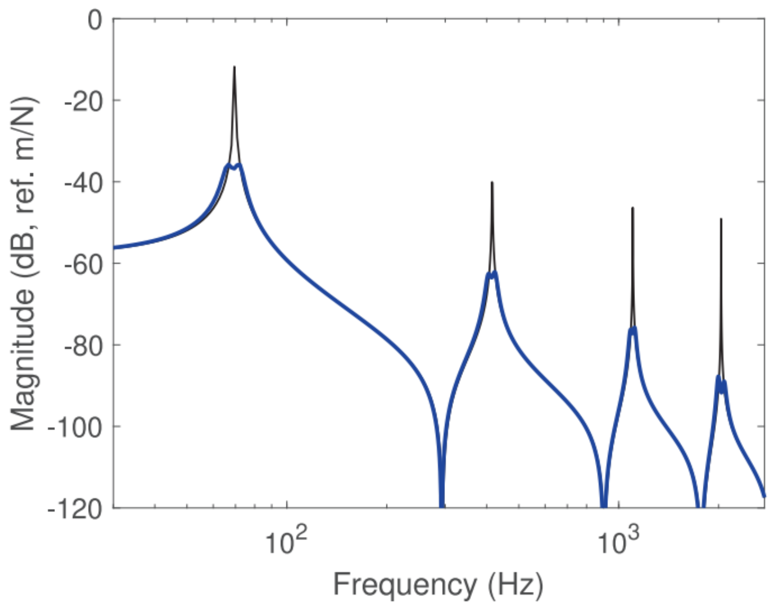

Figure 6: FRF for the first four modes where the black line represents the open-circuited patches, and the blue line represents the current blocking shunt [21].

2.2. Active Vibration Control

Active piezoelectric damping has drawn a great deal of attention in the field of structural engineering as an advanced vibration control approach. Active piezoelectric damping had a greater scope that went beyond the basic functionality of piezoelectric devices. Other damping control systems frequently fell short of providing the needed amount of vibration reduction, especially in settings with dynamic loads and unpredictable disturbances. Compared to passive systems, which are constrained by their physical attributes and are often made for particular frequency ranges. They are more efficient in a broader range of applications. They can achieve multimode vibration control because they can be instantly adapted in response to changing vibration frequencies and amplitudes in real time [27]. However, an external power source is not suitable for some applications. The external power source adds weight and complexity to the main structure, which is undesirable in many cases. Piezoelectric passive systems use shunted circuits to introduce damping to the system without needing an external power source. In contrast with passive methods, the active control approach doesn’t rely on a shunt circuit most of the time; piezoelectric transducers are utilized mainly as sensors or actuators in active vibration control and other applications. A reconstruction of the internal piezoelectric strain voltage can be produced by subtracting the capacitive voltage drop from the applied terminal voltage. This approach is now known as piezoelectric self-sensing. The reconstructed strain voltage can be used as an active feedback sensor, eliminating the necessity for an additional transducer [28,29].

Several researchers have worked on introducing an active electrical component to the shunted circuit, Forward [30] proposed using an active electronic circuit to reduce the capacitance of the transducer artificially, thereby increasing the mechanical energy-to-electric energy conversion rate. One of the most used active elements is the negative capacitor. Negative capacitors are commonly used to counteract the positive capacitance that is intrinsic to piezoelectric materials. The capacitance of piezoelectric transducers frequently limits the frequency response and effectiveness of standard passive vibration control systems. Nevertheless, implementing a negative capacitor in the circuit significantly overcomes these constraints. The shunt circuit that contains a negative capacitor demonstrates improved capabilities for energy transfer and dissipation, which ultimately contribute to more efficient vibration suppression over a broader frequency spectrum [31].

The implementation of a negative capacitance controller in active vibration attenuation is investigated by Behrens et al. [32]. An experimental and theoretical analysis of the controller's effect on a piezoelectric laminated structure is provided. It is demonstrated that the active shunt negative capacitance controller effectively dampens multiple vibration modes. It is less sensitive to environmental changes, easier to implement, and functions as a broad-spectrum vibration absorber. The paper shows the effectiveness of this method in damping the first six vibration modes, as shown in Figure 7 and illustrates its advantages in comparison to passive methods.

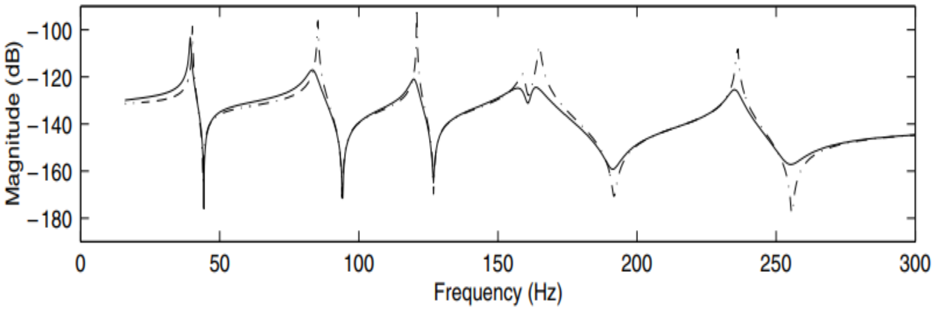

Figure 7: FRF for the first 6 modes, the dashed line is the undamped condition, and the solid line is the damped condition [32].

Park and Park [33] proposed an innovative shunt circuit that utilizes piezoceramic patches to attenuate multi-mode vibration amplitudes. The characteristics of piezoelectric dampers connected in series and parallel to resistor-negative capacitor branch circuits are investigated, as shown in Figure 8. The model used Hamilton's principle to formulate governing equations of motion for a piezo/beam system incorporating negative capacitive shunting. The theoretical analysis provides evidence that this system is capable of significantly minimizing the amplitudes of multiple-mode vibrations throughout the entire frequency range of the structure.

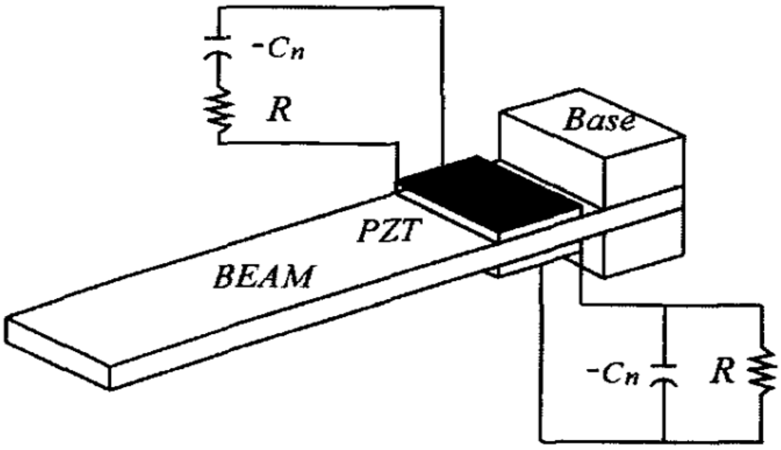

Figure 8: Schematic drawing of a resistor-negative capacitor in series or parallel coupled with a cantilever beam by a piezoelectric patch [33].

Benjamin et al. [34] concentrated their efforts on employing shunted piezoelectric patches to mitigate vibrations in a stiffened airplane panel. They investigate the ability of negative capacitance shunts to suppress vibrations throughout a wide frequency range. Using numerical models and experimental research, the study evaluates how well negative capacitance shunts reduce vibrations in complicated structures, specifically a stiffened airplane test panel. The outcomes show this method's potential for actual vibration control applications.

2.3. Semi-active Vibration Control

In order to operate actuators, an active control system often needs powerful power amplifiers and high-performance digital signal processors, which are unsuitable for space applications. While passive control systems are easier to implement than active control systems, they are less robust to system disturbances. Semi-active control systems, also known as semi-active systems, have attracted a lot of interest in providing vibration damping effectively utilizing piezoelectric materials. These systems offer an adaptable way to reduce vibrations in various applications by combining the advantages of adaptability and energy efficiency. In the context of shunt circuit vibration control, semi-active systems need a supply of external energy to actively modify system characteristics such as damping and stiffness. While this offers great accuracy in vibration reduction control, it also reduces system complexity and energy consumption in comparison to fully active systems [35].

Clark [36] proposed a semi-active control method for mechanical systems that uses state-switched piezoelectric actuators. To store and release energy as needed, the piezoelectric actuator switches between an open-circuit, short-circuit, or resistive-circuit state. The control law for state-switching is derived from the system's motion with respect to its equilibrium. As the system deviates from equilibrium, the circuit transitions to a high-stiffness condition, where it becomes an open circuit. On the other hand, when the system is approaching a condition of balance, it is transitioned to a state of low stiffness and dissipation (such as a short or resistive circuit). Comparing the OC-SC system's damped impulse response to that of the RS system and the OC-RS system as demonstrated in Figure 9.

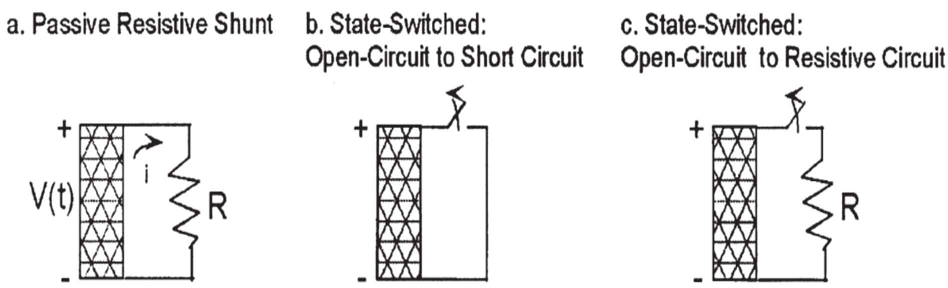

Figure 9: Three circuit configurations that are used in the study [37].

The outcome of the numerical simulation reveals that the passive-resistive shunt circuit offers slightly greater damping, as demonstrated in Figure 10. The state-switched systems, however, are less sensitive to changes in actuator material compliance and mass. Additionally, the state-switched systems work well in the low-frequency range, where stiffness dominates, according to harmonic response analysis, making them a suitable substitute for active control systems.

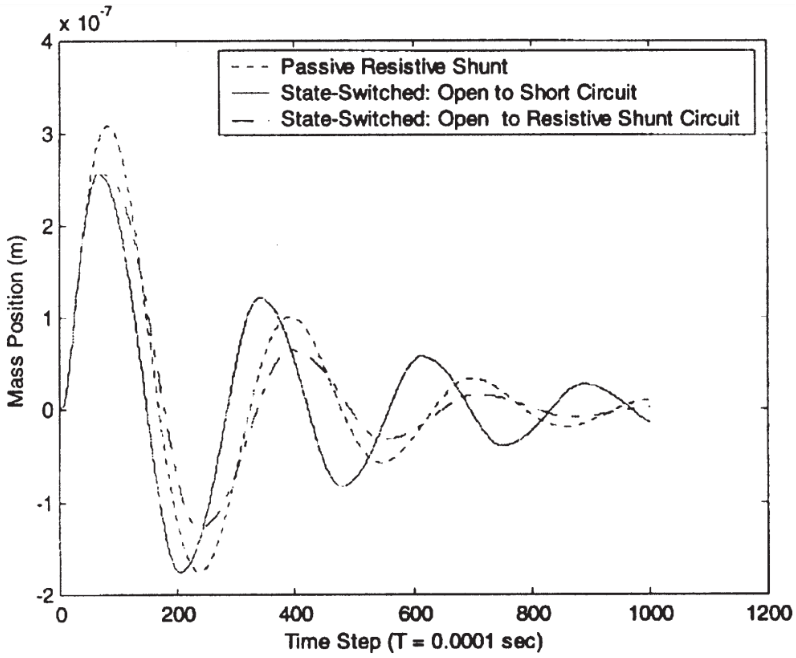

Figure 10: The time response from impulse excitation for three cases [37].

The Synchronized Switch Damping (SSD) method for resonance damping in mechanical systems is presented by Richard et al. [37]. With this semi-active technique, a piezoelectric device is continuously switched from open to short circuit in time with the motion of the structure. Energy dissipation results from this transition because it causes a phase shift between voltage and piezoelectric strain. One new feature is that the piezoelectric device is connected to a small inductor to improve damping and optimize voltage amplitude instead of discharging during a short circuit. With the exception of the switch device's low-power circuitry, the technique works at any frequency and doesn't require a huge inductor for low frequencies. It also doesn't require an external power source. Significant improvements in damping have been shown in experimental results on a variety of material beams.

Lefeuvre et al. [38] presented an improved semi-active damping technique (SSDV). Optimizing the damping of structural vibrations, this technique synchronizes the switching of a piezoelectric device with voltage sources. The methodology enhances the effectiveness of energy dissipation and structural attenuation by artificially augmenting the voltage's amplitude. Resonant cantilever beams exhibit considerable vibration attenuation, as demonstrated by both theoretical predictions and experimental findings.

A novel semi-active multi-modal vibration control method utilizing a piezoceramic actuator combined with a switching resistor/inductor shunt is presented by Corr and Clarck [39]. Applying a signed charge for energy dissipation through timing-based shunt switching based on the rate of energy change in controlled modes is the technique's method. Several structures are subjected to numerical and experimental tests, demonstrating the effectiveness of this approach in dissipating energy in several modes with a single actuator, as shown in Figure 11.

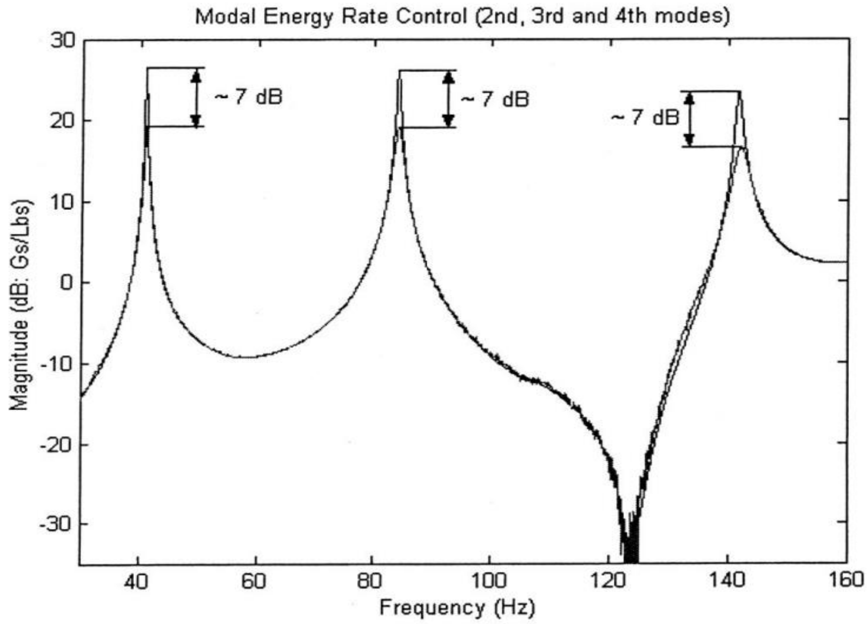

Figure 11: FRF of the mechanical energy dissipation for 2nd, 3rd and 4th modes [39].

By using a self-sensing method based on nonlinear synchronized switch damping on negative capacitance (SSDNC). Wei et al. [40] presented a novel method for semi-active vibration control. The suggested method offers a more straightforward and reliable method, eliminating the need for external sensors and controls. The experiments examined the self-sensing SSDNC technique's dampening capabilities by changing the negative capacitance values. The outcomes showed how well the suggested method mitigates vibration, with better results shown when the negative capacitance is raised. Additionally, various negative capacitance (NC) values in the saturation area showed that the damping performance would improve with a higher power supply voltage.

2.4. Exploiting Internal Resonances in Vibration Absorbers

The use of internal resonances in vibration damping was first proposed by Hacton and Barr [41] in which their passive vibration damper is a nonlinear autoparametric absorber that works based on internal resonance. Their approach relies on connecting the single-degree-of-freedom system to a cantilever beam with a tip mass. After forcing the system to resonance, they discovered that the absorber could efficiently limit and create a threshold for the amplitude of oscillations of the main mass by tuning the beam and the other system frequencies.

Moreover, most of the researchers have used internal resonance in active control systems [42,43]. Utilizing two-to-one internal resonances and quadratic nonlinearities, Oueini et al. [44] presented a novel active nonlinear vibration absorber for flexible structures. The method used sensors and actuators to connect second-order controllers to a cantilever beam. Using strain gauges for feedback and piezoceramic patches for actuation, as shown in Figure 12, it is the first internal resonance vibration absorption system to use piezoelectric materials.

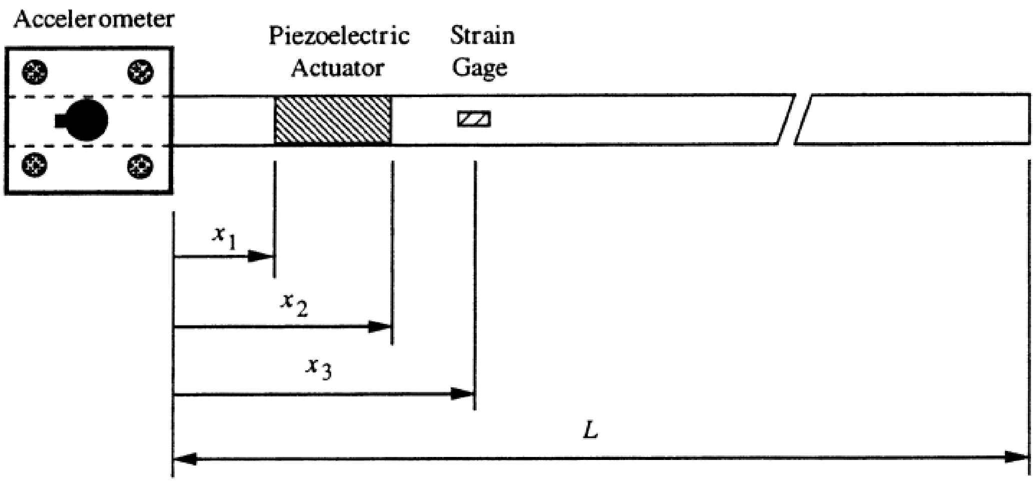

Figure 12: the implementation of piezoelectric actuators and sensors on a cantilever beam [44].

A semi-active nonlinear vibration attenuation approach is proposed by Shami et al. [45]. A quadratic nonlinearity was added to a shunted circuit to be tuned to obtain a 2:1

internal resonance between the mechanical resonance and the electrical resonance. This created a nonlinear antiresonance and a saturation phenomenon, thus allowing the mechanical amplitude to be independent of the forcing amplitude above a threshold. The tuning of the nonlinear parameters of the shunted circuit has been studied and optimized. Two scenarios have been numerically tested and are shown in Figure 13. One with a nonlinear capacitor (a) that depends on charge amplitude, and the other is a voltage source (b) that is proportional to the square of the voltage produced by the piezoelectric element. This is the only work that has been done regarding the use of internal resonance in shunted circuits.

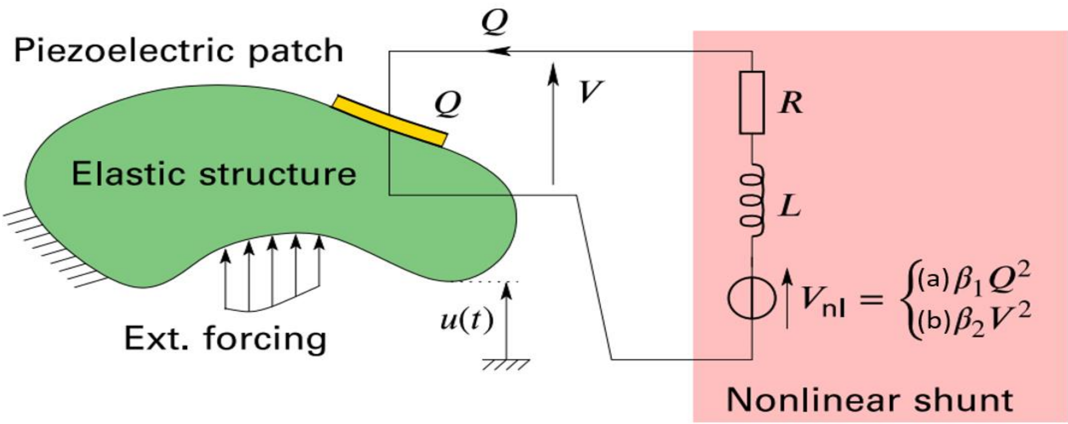

Figure 13: Nonlinear shunt circuit coupled to a structure by piezoelectric patches [45].

Chapter 3. Model

The objective of this chapter is to improve structural damping using an in-depth methodology that includes modal analysis, electromechanical coupling, and internal resonance. To begin with, a full modal analysis of the structure will be undertaken to understand its dynamic properties better. The structure will then be coupled with a shunted circuit via piezoelectric materials, exploiting their electromechanical capabilities for energy dissipation. To improve damping, this crucial stage involves implementing and controlling internal resonance inside the system. Also, the same procedure will be done on a nonlinear structure to demonstrate the coupling between the shunted circuit and a nonlinear cantilever beam, a mathematical model representing this relationship and demonstrating the internal resonance will be formulated at the end of this chapter.

3.1. Modal Analysis of a Cantilever Beam.

The governing equation for the linear harmonically excited vibration of an Euler-Bernoulli beam is

$$m\frac{\partial^2 u}{\partial t^2} + EI\frac{\partial^4 u}{\partial x^4} = F(x)\cos(\Omega t) \tag{1}$$

Where $u(x,t)$ is the lateral deflection, E, I, and m are, respectively, the modules of elasticity, the second moment of area, and the mass per unit length of the beam. F(x) is the applied force distribution and Ω is its frequency. The deflection of the beam is approximated as

$$u(x,t) = \varphi(x)\, e^{j\omega t} \tag{2}$$

Where $\varphi(x)$ is the mode shape. The boundary conditions of the cantilever beam are as follows:

$$u = 0, \qquad \frac{\partial u}{dx} = 0 \qquad at\ x = 0 \tag{3}$$

$$\frac{\partial^2 u}{\partial x^2} = 0, \qquad \frac{\partial^3 u}{\partial x^3} = 0 \qquad at\ x = l \tag{4}$$

By using the boundary conditions for solving the Euler-Bernoulli equation, the mode shapes can be derived as

$$\varphi_i(x) = \sin(K_i x) - \sinh(K_i x) - \sigma(\cos(K_i x) - \cosh(K_i x)) \tag{5}$$

$$\sigma = \frac{\sinh(K_i l) + \sin(K_i l)}{\cosh(K_i l) + \cos(K_i l)} \tag{6}$$

For consistency and simplicity, we are going to non-dimensionalize the mode shape with respect to the beam length by assuming $\zeta = \frac{x}{l}$, where the mode shape becomes

$$\varphi(\zeta) = \sin(K_i \zeta) - \sinh(K_i \zeta) - \sigma(\cos(K_i \zeta) - \cosh(K_i \zeta)) \tag{7}$$

$$\sigma = \frac{\sinh(K_i) + \sin(K_i)}{\cosh(K_i) + \cos(K_i)} \tag{8}$$

To obtain the natural frequencies, $the\ K$ values for several modes are derived from the following characteristic equation:

$$cosh(K_i) * cos(K_i) + 1 = 0 \tag{9}$$

The constant K_i for the first 5 modes is equal to 1.875, 4.694, 7.855, 10.995, and 14.137, respectively. After defining the mode shape, the lateral deflection of the beam is going to be defined as

$$u(\zeta, t) = \varphi(\zeta) \times q(t) \tag{10}$$

Substituting Eq. (10) into Eq. (1), the discretized equation is obtained as follows:

$$m \sum_{i=1}^{N} \ddot{q}_i(t)\varphi_i(\zeta) + EI \sum_{i=1}^{N} q_i(t)\varphi_i''''(\zeta) = F \cos \Omega t \tag{11}$$

Galerkin's method is used to discretize the governing equation by multiplying Eq. (11) by a mode shape φ_j and integrating over the domain

$$m \int_0^1 \sum_{i=1}^{N} \varphi_i(\zeta) \times \ddot{q}_i(t) \times \varphi_j(\zeta)\, d\zeta$$
$$+ EI \int_0^1 \sum_{i=1}^{N} \varphi_i''''(\zeta) \times q_i(t) \times \varphi_j(\zeta)\, d\zeta = \int_0^1 F(\zeta) \cos \Omega t \times \varphi_j(\zeta) d\zeta \tag{12}$$

The solution of the free vibration defines the following orthogonality conditions:

$$\int_0^1 \varphi_j(\zeta) \times \varphi_i''''(\zeta)\, d\zeta = \begin{cases} K_i^4, & i = j \\ 0, & i \neq j \end{cases} \tag{13}$$

$$\int_0^1 \varphi_j(\zeta) \times \varphi_i(\zeta)\, d\zeta = \begin{cases} 1, & i = j \\ 0, & i \neq j \end{cases} \tag{14}$$

The resulting modal equations of the linear system after applying the orthogonality conditions on Eq. (12) are

$$\ddot{q}_i + \omega_i{}^2 q_i = f_i \cos \Omega t \tag{15}$$

Where the forcing term is $f_j = \frac{1}{m}\int_0^1 F(\zeta)\phi_j d\zeta$, and the ith mode natural frequency ω_i is defined as

$$\omega_i = \sqrt{\frac{EI}{ml^4}} K_i^2 \tag{16}$$

3.2. Coupling a Cantilever Beam with a Shunted Circuit

To control the vibration of a beam by a shunted circuit, the coupling between the beam, piezoelectric patch, and the circuit should be analyzed. Following Shami et al. [46], a set of coupled equations that represents the coupling between a cantilever beam and a passive shunted circuit is derived. The equations represent the beam, piezoelectric patch, and the circuit are, respectively, given as

$$\ddot{q}_i + \omega_i{}^2 q_i + K_c V = f_i\, cos(\Omega t) \tag{17}$$

$$C_p V - Q - K_c q_i = 0 \tag{18}$$

$$V + L\ddot{Q} + R\dot{Q} + V_{nl} = 0 \tag{19}$$

Where the parameters are defined as follows: K_c is the coupling factor of the piezoelectric patch, C_p is the capacitance of the piezoelectric patch, and V and Q represent the voltage and electrical charges, respectively, L and R are the inductance and resistance of the RL shunted circuit. The voltage in Eq. (18) will be substituted in Eq. (17) and Eq. (19) to couple the shunted circuit directly to the structure, optimizing the circuit elements and studying their contribution to vibration damping.

$$\ddot{q}_i + \left(\omega_i{}^2 + \frac{K_c^2}{C_p}\right) q_i + \frac{K_c}{C_p} Q = f_i\, cos(\Omega t) \tag{20}$$

$$\ddot{Q} + 2\zeta_e \omega_e \dot{Q} + \omega_e^2 Q + \frac{K_c}{LC_p} q_i = 0 \tag{21}$$

Where the electrical natural frequency and electrical damping ratio are defined as

$$\omega_e = \frac{1}{\sqrt{LC_p}} \tag{22}$$

$$\zeta_e = \frac{R}{2}\sqrt{\frac{C_p}{L}} \tag{23}$$

Investigating Eq. (20), the effective natural frequency is defined as follows:

$$\widehat{\omega}_i^2 = \omega_i{}^2 + \frac{K_c^2}{C_p} \tag{24}$$

Introducing modal damping into the structural equation of motion, the governing equations of the system are represented by

$$\ddot{q}_i + 2\zeta_i\widehat{\omega}_i\dot{q}_i + \widehat{\omega}_i^2 q_i + \frac{K_c}{C_p}Q = f_i\, cos(\Omega t) \tag{25}$$

$$\ddot{Q} + 2\zeta_e\omega_e\dot{Q} + \omega_e^2 Q + \frac{K_c}{LC_p}q_i = 0 \tag{26}$$

3.3. Inducing Internal Resonances into the System

The internal resonance depends on the coupling between two modes that have nonlinearity with an integer ratio between their natural frequencies. To introduce a 2:1 internal resonance, the modes should have a quadratically nonlinear coupling. Nonlinearity can be induced in active systems by quadratic feedback and control signals [44]. Also, nonlinearity can be induced in passive and semi-active systems by using nonlinear electrical components such as nonlinear capacitors in which its capacitance depends inversely on the amplitude of the charge. The implementation of the nonlinear capacitor to the shunted circuit can be represented as

$$C_{nl} = \frac{1}{Q} \tag{27}$$

$$V_{nl} = N\frac{Q}{C_{nl}} = NQ^2 \tag{28}$$

Where Eq. (19) becomes

$$\ddot{Q} + 2\zeta_e \omega_e \dot{Q} + \omega_e^2 Q + \frac{K_c}{LC_p} q + \frac{N\, Q^2}{L} = 0 \tag{29}$$

To demonstrate the design of the proposed model, Figure 14 presents the cantilever beam (structure), the piezoelectric patch (transducer), and the shunted circuit (absorber). The components of the circuit are the resistor, the inductor, and the nonlinear capacitor that will create the internal resonance.

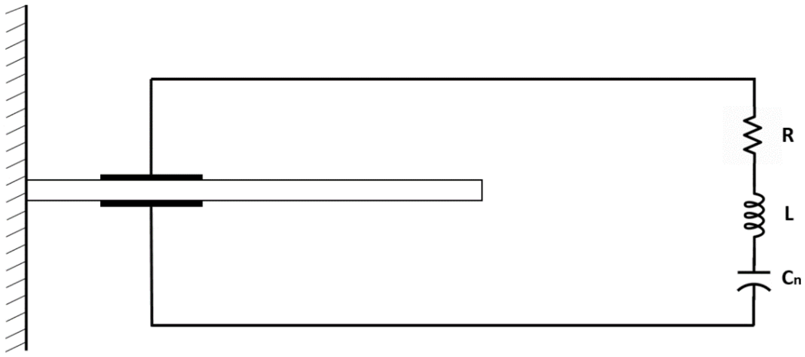

Figure 14: A cantilever beam coupled with a shunted circuit that has a nonlinear capacitor.

It's obvious that the coupling terms in the system are not the same as shown in Eqs. (25-26). Therefore, we are going to define the following dimensionless parameters to unify the coupling term:

$$\tau = \hat{\omega}_1 t\,, \qquad \tilde{q} = q\,, \qquad \tilde{Q} = \sqrt{L}\, Q, \qquad \tilde{\Omega} = \frac{\Omega}{\hat{\omega}_1} \tag{30}$$

The open-circuit natural frequency of the ith structural mode after connecting it to the circuit is

$$\hat{\omega}_i = \sqrt{\omega_i^2 + \frac{K_c^2}{C_p}} \tag{31}$$

Substituting the nondimensional parameters into the system of equations, we obtain

$$\ddot{\tilde{q}}_i + 2\zeta_i \dot{\tilde{q}}_i + \tilde{q}_i + \frac{K_c}{\hat{\omega}_1^2 C_p \sqrt{L}} \tilde{Q} = \frac{f_i}{\hat{\omega}_1^2} \cos\left(\tilde{\Omega}\tau\right) \tag{32}$$

$$\ddot{\tilde{Q}} + 2\zeta_e \omega_r\, \dot{\tilde{Q}} + \omega_r^2 \tilde{Q} + \frac{K_c}{\hat{\omega}_1^2 C_p \sqrt{L}} \tilde{q}_i + \frac{N \tilde{Q}^2}{L^{\frac{3}{2}} \hat{\omega}_1^2} = 0 \tag{33}$$

To simplify the notations, the hat (~) will be omitted and the derivatives take place with the nondimensional time. The internal resonance phenomena don't appear in Eq. (32) and Eq. (33) that are in the physical co-ordination because they are coupled linearly, so a modal analysis is required to transform the equations into the modal co-ordination where modal coupling between the mechanical mode and electrical mode can be observed since the properties of the internal resonance are directly linked to the modal co-ordinates. For the modal analysis, first, we have to assume the model to be free, linear, and undamped

$$\ddot{q}_i + q_i + \alpha\, Q = 0 \tag{34}$$

$$\ddot{Q} + \omega_r^2\, Q + \alpha\, q_i = 0 \tag{35}$$

Where

$$\alpha = k_i \omega_r = \frac{K_c}{\widehat{\omega}_1^2 C_p \sqrt{L}} \tag{36}$$

And ω_r is the frequency ratio and k_i is the electromechanical coupling factor

$$\omega_r = \frac{\omega_e}{\widehat{\omega}_1} \tag{37}$$

$$k_i = \frac{K_c}{\widehat{\omega}_1 \sqrt{C_p}} \tag{38}$$

Rearranging Eqs. (34-35) in a matrix form yields

$$\begin{bmatrix} 1 & 0 \\ 0 & 1 \end{bmatrix} \begin{pmatrix} \ddot{q} \\ \ddot{Q} \end{pmatrix} + \begin{bmatrix} 1 & \alpha \\ \alpha & \omega_r^2 \end{bmatrix} \begin{pmatrix} q \\ Q \end{pmatrix} = \begin{pmatrix} 0 \\ 0 \end{pmatrix} \tag{39}$$

By letting

$$\tilde{q}_i = C_1 e^{j\omega t} \tag{40}$$

$$\tilde{Q} = C_2 e^{j\omega t} \tag{41}$$

And solving for the eigenvalues ω

$$\left[[K] - \omega^2 [I]\right] \begin{bmatrix} C_1 \\ C_2 \end{bmatrix} = \begin{bmatrix} 0 \\ 0 \end{bmatrix} \tag{42}$$

$$\begin{vmatrix} 1-\omega^2 & \alpha \\ \alpha & {\omega_r}^2-\omega^2 \end{vmatrix} = 0 \tag{43}$$

The eigenvalues are obtained as follows:

$${\omega_1}^2 = \frac{(1+\omega_r^2)-\sqrt{(1+\omega_r^2)^2-4(\omega_r^2-\alpha^2)}}{2} \tag{44}$$

$${\omega_2}^2 = \frac{(1+\omega_r^2)+\sqrt{(1+\omega_r^2)^2-4(\omega_r^2-\alpha^2)}}{2} \tag{45}$$

Now to calculate the eigenvectors, we substitute Eqs. (44) and (45) into Eq. (43)

$$\begin{bmatrix} 1-\dfrac{(1+\omega_r^2)\pm\sqrt{\varphi}}{2} & \alpha \\ \alpha & {\omega_r}^2-\dfrac{(1+\omega_r^2)\pm\sqrt{\varphi}}{2} \end{bmatrix} \begin{bmatrix} C_1 \\ C_2 \end{bmatrix} = 0 \tag{46}$$

$$\varphi = (1+\omega_r^2)^2 - 4(\omega_r^2-\alpha^2) \tag{47}$$

The eigenvectors are obtained as follows:

$$V_1 = \beta_1 \begin{bmatrix} -\theta \\ 1 \end{bmatrix} \tag{48}$$

$$V_2 = \beta_2 \begin{bmatrix} 1 \\ \theta \end{bmatrix} \tag{49}$$

Where θ is equal to

$$\theta = \frac{2\alpha}{1-\omega_r^2+\sqrt{(1+\omega_r^2)^2-4(\omega_r^2-\alpha^2)}} \tag{50}$$

By the orthogonality condition

$$V^T I V = 1 \tag{51}$$

$$\beta_1 = \beta_2 = \sqrt{\frac{1}{\theta^2+1}} \tag{52}$$

The eigenvector matrix can be arranged as follows:

$$\phi = \begin{bmatrix} -\theta\sqrt{\dfrac{1}{\theta^2+1}} & \sqrt{\dfrac{1}{\theta^2+1}} \\ \sqrt{\dfrac{1}{\theta^2+1}} & \theta\sqrt{\dfrac{1}{\theta^2+1}} \end{bmatrix} \tag{53}$$

For the transformation from the physical coordinates to the principal coordinates, the expansion theorem is utilized

$$\begin{pmatrix} q \\ Q \end{pmatrix} = (\phi)\begin{pmatrix} x_1 \\ x_2 \end{pmatrix} \tag{54}$$

By substituting Eq. (54) into Eq. (32) and Eq. (33), and pre-multiplying by ϕ^T, the modal system of equations becomes

$$\begin{bmatrix} 1+\theta^2 & 0 \\ 0 & 1+\theta^2 \end{bmatrix}\begin{bmatrix} \ddot{x}_1 \\ \ddot{x}_2 \end{bmatrix} + \begin{bmatrix} 2\zeta_i\theta^2 + 2\zeta_e\omega_r & -2\zeta_i\theta + 2\zeta_e\omega_r\theta \\ -2\zeta_i\theta + 2\zeta_e\omega_r\theta & 2\zeta_i + 2\zeta_e\omega_r\theta^2 \end{bmatrix}\begin{bmatrix} \dot{x}_1 \\ \dot{x}_2 \end{bmatrix}$$

$$+\begin{bmatrix} \theta^2 - 2\theta\alpha + \omega_r^2 & -\theta - \alpha\theta^2 + \theta\omega_r^2 + \alpha \\ -\theta - \alpha\theta^2 + \theta\omega_r^2 + \alpha & 1 + 2\alpha\theta + \theta\omega_r^2 \end{bmatrix}\begin{bmatrix} x_1 \\ x_2 \end{bmatrix}$$

$$+\begin{bmatrix} \dfrac{N}{\sqrt{L^3}\,\widehat{\omega}_1^2} & \dfrac{2N\theta}{\sqrt{L^3}\,\widehat{\omega}_1^2} & \dfrac{N\theta^2}{\sqrt{L^3}\,\widehat{\omega}_1^2} \\ \dfrac{\theta N}{\sqrt{L^3}\,\widehat{\omega}_1^2} & \dfrac{2N\theta^2}{\sqrt{L^3}\,\widehat{\omega}_1^2} & \dfrac{N\theta^3}{\sqrt{L^3}\,\widehat{\omega}_1^2} \end{bmatrix}\begin{bmatrix} x_1^2 \\ x_1x_2 \\ x_2^2 \end{bmatrix} = \begin{bmatrix} -\theta\dfrac{f_i}{\widehat{\omega}^2}\,cos(\widetilde{\Omega}\tau) \\ \dfrac{f_i}{\widehat{\omega}^2}\,cos(\widetilde{\Omega}\tau) \end{bmatrix}$$

The value of θ is considered to be small, therefore we are going to assume $\theta^2 \approx 0$. The nonlinear coupled equations that represent the system are as follows:

$$\ddot{x}_1 + \xi_1\dot{x}_1 + \xi_2\dot{x}_2 + \omega_r^2 x_1 + \frac{N}{\sqrt{L^3}\,\widehat{\omega}_1^2}\,x_1^2 + \frac{2N\theta}{\sqrt{L^3}\,\widehat{\omega}_1^2}\,x_1x_2 + \frac{N\theta^2}{\sqrt{L^3}\,\widehat{\omega}_1^2}\,x_2^2 = -\theta\bar{F} \tag{55}$$

$$\ddot{x}_2 + \xi_2\dot{x}_1 + \xi_3\dot{x}_2 + x_2 + \theta\,\frac{N}{\sqrt{L^3}\,\widehat{\omega}_1^2}\,x_1^2 + \frac{2N\theta^2}{\sqrt{L^3}\,\widehat{\omega}_1^2}\,x_1x_2 + \frac{N\theta^3}{\sqrt{L^3}\,\widehat{\omega}_1^2}\,x_2^2 = \bar{F} \tag{56}$$

Were after subsitiuting θ and α, the stifness matrix became a diagonal matrix of ω_r^2 and 1 Representing the electrical and mechanical natural frequencies respectively with devided by the mechanical frequency. We defined the following parameters to simplify the equations above:

$$\bar{F} = \frac{f}{\bar{\omega}_1^2} cos(\tilde{\Omega}\tau),\ \xi_1 = 2\zeta_1\theta^2 + 2\zeta_e\omega_r,\ \xi_2 = -2\zeta_1\theta + 2\zeta_e\omega_r\theta,\ \ \xi_3 = 2\zeta_1 + 2\zeta_e\omega_r\theta^2$$

3.4. Adding the Structural Nonlinearity

In the previous section, we demonstrated the implementation of a shunted circuit on a linear cantilever beam to damp vibrations through internal resonance. Expanding upon the existing knowledge, the present section explores the complex field of nonlinear structures. Vibration control in nonlinear systems is challenging due to their distinctive nonlinear dynamic responses to external excitations. Nonlinear systems differ from linear systems in that the relationship between applied forces and resulting displacements is not straightforward. Nonlinear systems reveal behaviors like amplitude-dependent frequencies, which add complexity to their vibration mitigation.

To study the performance of the absorber under the influence of other nonlinear effects related to the structure, we will investigate how the absorber deals with the nonlinearity that comes from the nonplanar oscillations presented by Arafat et al [47]. The nonplanar oscillations are caused by geometric nonlinearities and inertia nonlinearities. In particular, nonlinearity arises from the coupling of flexural and torsional motions that are caused by large deformation**.** To account for the nonlinearity, we follow Arafat et al. [47], therefore, we are going to end up with the following equation of motion for the nonlinear structure:

$$EIu'''' + m\ddot{u} + \frac{m}{2}\left\{ u' \int_1^\zeta \frac{\partial^2}{\partial t^2}\ \left[\int_0^\zeta (u')^2\, d\zeta\right] d\zeta \right\}' + EI[u'(u'u'')']' \\ = F(x)\cos(\Omega t) \tag{57}$$

Where the displacement u is expanded as follows:

$$u(\zeta, t) = \varphi(\zeta)\, q(t) \tag{58}$$

For the discretization, Eq. (58) will be substituted in Eq. (57). The equation of motion of a free cantilever beam accounting for the geometric/inertia nonlinearities becomes

$$EI\varphi''''(\zeta)q(t) + m\varphi(\zeta)\ddot{q}(t) + \frac{m}{2}\left\{\varphi'(\zeta)q(t)\int_1^\zeta \frac{\partial^2}{\partial t^2}\ \left[\int_0^\zeta \left(\varphi'(\zeta)q(t)\right)^2 d\zeta\right] d\zeta\right\}' \\ +EI\left[\ \varphi'(\zeta)q(t)\left(\varphi'(\zeta)\varphi''(\zeta)q^2(t)\right)'\right]' = F(x)\cos(\Omega t) \tag{59}$$

For the discretization of the equation, we followed the same procedure in Section 3.1 with the non-dimensionalizing and the assumption of a free-linear-undamped structure to derive the mode shape and the eigenfrequencies. Once we have added the nonlinear, and excitation terms, we can apply the Galerkin's method to obtain the following equation:

$$EI\int_0^1 \sum_{i=1}^{N} \varphi_i''''(\zeta) \times q_i(t) \times \varphi_j(\zeta)\ d\zeta + m\int_0^1 \sum_{i=1}^{N} \varphi_i(\zeta) \times\ \ddot{q}_i(t) \times \varphi_j(\zeta)\, d\zeta$$

$$+\frac{m}{2}\int_0^1 \left\{\varphi'(\zeta)q(t)\int_1^\zeta \frac{\partial^2}{\partial t^2}\ \left[\int_0^\zeta \big(\varphi'(\zeta)q(t)\big)^2 d\zeta\right] d\zeta\right\}'\ \varphi(\zeta)\, d\zeta$$

$$+EI\ \int_0^1 \left[\ \varphi'(\zeta)q(t)\ \big(\varphi'(\zeta)\varphi''(\zeta)q^2(t)\big)'\right]'\ \varphi(\zeta)$$

$$= \int_0^1 Fcos(\Omega t)\varphi(\zeta)\ d\zeta \tag{60}$$

Following the orthogonality conditions mentioned in Eq. (13) and Eq. (14), the equation of motion will be

$$\ddot{q}_i + \omega_i^2 q_i$$

$$+\frac{1}{2}\int_0^1 \left\{\varphi'(\zeta)q(t)\int_1^\zeta \frac{\partial^2}{\partial t^2}\ \left[\int_0^\zeta \big(\varphi'(\zeta)q(t)\big)^2 d\zeta\right] d\zeta\right\}'\ \varphi(\zeta)\, d\zeta$$

$$+\frac{EI}{m}\ \int_0^1 \left[\ \varphi'(\zeta)q(t)\ \big(\varphi'(\zeta)\varphi''(\zeta)q^2(t)\big)'\right]'\ \varphi(\zeta)$$

$$= \frac{1}{m}\int_0^1 Fcos(\Omega t)\varphi(\zeta)\ d\zeta \tag{61}$$

The first nonlinear term in Eq. (61) is known as a nonlinear inertia term, which is weak and does not contribute to the first mode. It also has an extremely small coefficient, as demonstrated in the following equation:

$$\frac{1}{2l^2}\int_0^1 \left\{\varphi'(\zeta)q(t)\int_1^\zeta \frac{\partial^2}{\partial t^2}\ \left[\int_0^\zeta \big(\varphi'(\zeta)q(t)\big)^2 d\zeta\right] d\zeta\right\}'\ \varphi(\zeta)\, d\zeta$$

$$= \frac{7.1055 \times 10^{-15}}{l^2}\ (\ddot{q}q^2 + \dot{q}^2 q) \tag{62}$$

Therefore, we will exclude this term from the equation of motion. On the other hand, the other nonlinear term is considered a geometric nonlinearity, which is dominant in the first mode, and it's kept in the equation as follows:

$$\frac{EI}{m}\int_0^1 \left[\varphi'(\zeta)q(t)\left(\varphi'(\zeta)\varphi''(\zeta)q^2(t)\right)'\right]'\varphi(\zeta) = \frac{40.477EI}{ml^6}q^3 = Cq^3 \tag{63}$$

After applying the Galerkin's procedure, the system of discretized equations considering a single-mode approximation becomes

$$\ddot{q} + \omega_1^2 q + Cq^3 = f * \cos(\Omega \mathrm{t}) \tag{64}$$

Where the forcing term is $f = \frac{1}{m}\int_0^1 F(\zeta)\phi_1 d\zeta$. The coupled system of equations that represents the structure, piezoelectric patch, and the circuit will be

$$\ddot{q} + 2\zeta_1\omega_1\dot{q} + \omega_1^2 q + Cq^3 + K_c V = f\cos(\Omega \mathrm{t}) \tag{65}$$

$$C_p V - Q - K_c q = 0 \tag{66}$$

$$V + L\ddot{Q} + R\dot{Q} + V_{nl} = 0 \tag{67}$$

After coupling the equations of the structure and the circuit by using the equation of the patch, and also following the same non-dimensionalization in Section 3.3 by adding the modal damping**:**

$$\ddot{\tilde{q}}_i + 2\zeta_i\dot{\tilde{q}}_i + \tilde{q}_i + \frac{K_c}{\widehat{\omega}_1^2 C_p\sqrt{L}}\tilde{Q} + \frac{C}{\widehat{\omega}_1^2}\tilde{q}_i^3 = \frac{f_i}{\widehat{\omega}_1^2}\cos\left(\tilde{\Omega}\tau\right) \tag{68}$$

$$\ddot{\tilde{Q}} + \frac{2\zeta_e\omega_e}{\widehat{\omega}_1}\dot{\tilde{Q}} + \omega_r^2\tilde{Q} + \frac{K_c}{\widehat{\omega}_1^2 C_p\sqrt{L}}\tilde{q}_i + \frac{N\tilde{Q}^2}{L^{\frac{3}{2}}\widehat{\omega}_1^2} = 0 \tag{69}$$

For simplification, the hat (~) will be omitted. We will follow the same procedure of modal expansion to transfer the system from the physical coordinates to the modal coordinates as follows:

$$\begin{pmatrix} q \\ Q \end{pmatrix} = (\phi)\begin{pmatrix} x_1 \\ x_2 \end{pmatrix} \tag{70}$$

The system of equations that represents the system in the modal coordinates is given as:

$$\ddot{x}_1 + \xi_1\dot{x}_1 + \xi_2\dot{x}_2 + \omega_r^2 x_1 + \frac{N}{\sqrt{L^3}\,\widehat{\omega}_1^2}\,x_1^2 + \frac{2N\theta}{\sqrt{L^3}\,\widehat{\omega}_1^2}\,x_1x_2 + \frac{N\theta^2}{\sqrt{L^3}\,\widehat{\omega}_1^2}\,x_2^2 + \frac{C\theta^4}{\widehat{\omega}_1^2}x_1^3$$

$$+\frac{3C\theta^3}{\widehat{\omega}_1^2}x_1^2x_2 + \frac{3C\theta^2}{\widehat{\omega}_1^2}x_1x_2^2 + \frac{C\theta}{\widehat{\omega}_1^2}x_2^3 = -\theta\bar{F} \tag{71}$$

$$\ddot{x}_2 + \xi_2\dot{x}_1 + \xi_3\dot{x}_2 + x_2 + \frac{N\theta}{\sqrt{L^3}\,\widehat{\omega}_1^2}\,x_1^2 + \frac{2N\theta^2}{\sqrt{L^3}\,\widehat{\omega}_1^2}\,x_1x_2 + \frac{N\theta^3}{\sqrt{L^3}\,\widehat{\omega}_1^2}\,x_2^2 + \frac{C\theta^3}{\widehat{\omega}_1^2}x_1^3$$

$$+\frac{3C\theta^2}{\widehat{\omega}_1^2}x_1^2x_2 + \frac{3C\theta}{\widehat{\omega}_1^2}x_1x_2^2 + \frac{C}{\widehat{\omega}_1^2}\,x_2^3 = \bar{F} \tag{72}$$

3.5. The System Parameters

The chosen structure is a steel cantilever beam with the following characteristics:

Parameter:	Length (L)	Width (b)	Thickness (t)	Elastic modulus (E)	Density (ρ)
Value:	0.26 m	0.015 m	0.001 m	210 GPa	7850 Kg/m^3

Also, we are going to use soft PZT-P (Zr.Ti)O_3 C-82 as the material for the piezoelectric patches that has the following parameters [48]**:**

Parameter	Length (L_p)	Width (b_p)	Thickness (t_p)	Permittivity (ϵ^{T})	Piezoelectric charge coefficient (d_{31})
Numerical value	0.1 m	0.015 m	0.0005 m	3650	266×10^{-12} C/N

The natural frequencies are defined as

$$\omega_{\mathrm{i}} = \sqrt{\frac{EI}{\rho A L^4}}K_i^2 \tag{73}$$

Where their numerical values for the case in hand are

$$\omega_1 = 77.65 \frac{rad}{s}$$

$$\omega_2 = 486.65 \frac{rad}{s}$$

$$\omega_3 = 1362.8 \frac{rad}{s}$$

The capacitance of the piezoelectric patches is calculated by

$$C_p = \frac{2\epsilon^{\mathrm{T}}\epsilon^{\mathrm{o}} L_p b_p}{t_p} \tag{74}$$

$$C_p = 193.16\, nF$$

The nonlinear constant (N) that acts as a constant gain for the quadratic nonlinearity is defined as

$$N = 1 \times 10^{10}\, V/C^2$$

The piezoelectric coupling factor can be calculated for the first mode as follows [49]:

$$K_c = \frac{1}{m} \int_0^{L_p/L} 2 E_p d_{31} b_p \frac{t + t_p}{2} \Phi''(\zeta) \Delta H \, d\zeta \tag{75}$$

Where $\Delta H = H(\zeta - \zeta_1) - H(\zeta - \zeta_2)$ is the Heaviside function to locate the covered area by the piezoelectric patch. E_p is the Elastic modulus for piezoelectric material.

Chapter 4. Results and Analysis

This chapter summarizes the numerical results produced from studying the dynamic behaviors using the mathematical models that are derived in Chapter 3. This study considers two main cases: a linear structure and a nonlinear structure. Both structures are connected to a circuit that contains a nonlinear electrical element. This study aims to investigate the performance of internal resonance in different situations and presents a parametric analysis that guides the modeling of the electrical components in the circuit.

4.1. Electromechanical Coupling Factor (ECMF) Detuning Effect.

As seen in Eq. (75), the electromechanical coupling factor is determined by the interaction between the material characteristics of the piezoelectric patch and the components of the shunted circuit. The EMCF significantly impacts the frequency ratio (ω_r) as determined by Eq. (44) and Eq. (45). The effect appears in Figure 15a, illustrating a rapid and exponential increase of the deviation in the electromechanical frequency ratio as the EMCF increases. This observation is specific to a frequency ratio of 0.5. To create a 2:1 internal resonance in the system, the electromechanical frequency ratio must be set close to 0.5. Figure 15b demonstrates the variation of the frequency ratio with the electromechanical frequency ratio for four distinct EMCF values. For example, in a system with an EMCF of 0.2, the electromechanical frequency ratio required to induce internal resonance is 0.5175. This factor must be taken into account when modeling the shunted circuit and tweaking its electrical frequency.

4.2. Response of the Linear Structure Coupled with Shunted Circuit

Following the mathematical model that is developed in Section 3.3, the performance of the model is examined through numerical simulations. Figure 16 presents the time response of a cantilever beam with a piezoelectric patch positioned exactly at the beam's center. The figure displays the electrical mode amplitude, which represents the absorber, and the mechanical mode amplitude, which represents the structure. The cantilever beam is subjected to an excitation force of 0.5 N. Additionally, the circuit element parameters are set as follows: L=3470 H, R=3500 Ω, and N=1×10^{10}. These parameters are chosen as reference values for the circuit and to achieve a frequency ratio of 0.5 with the structure. The time response shows how the mechanical mode (structure) interacts with the electrical mode (Absorbers).

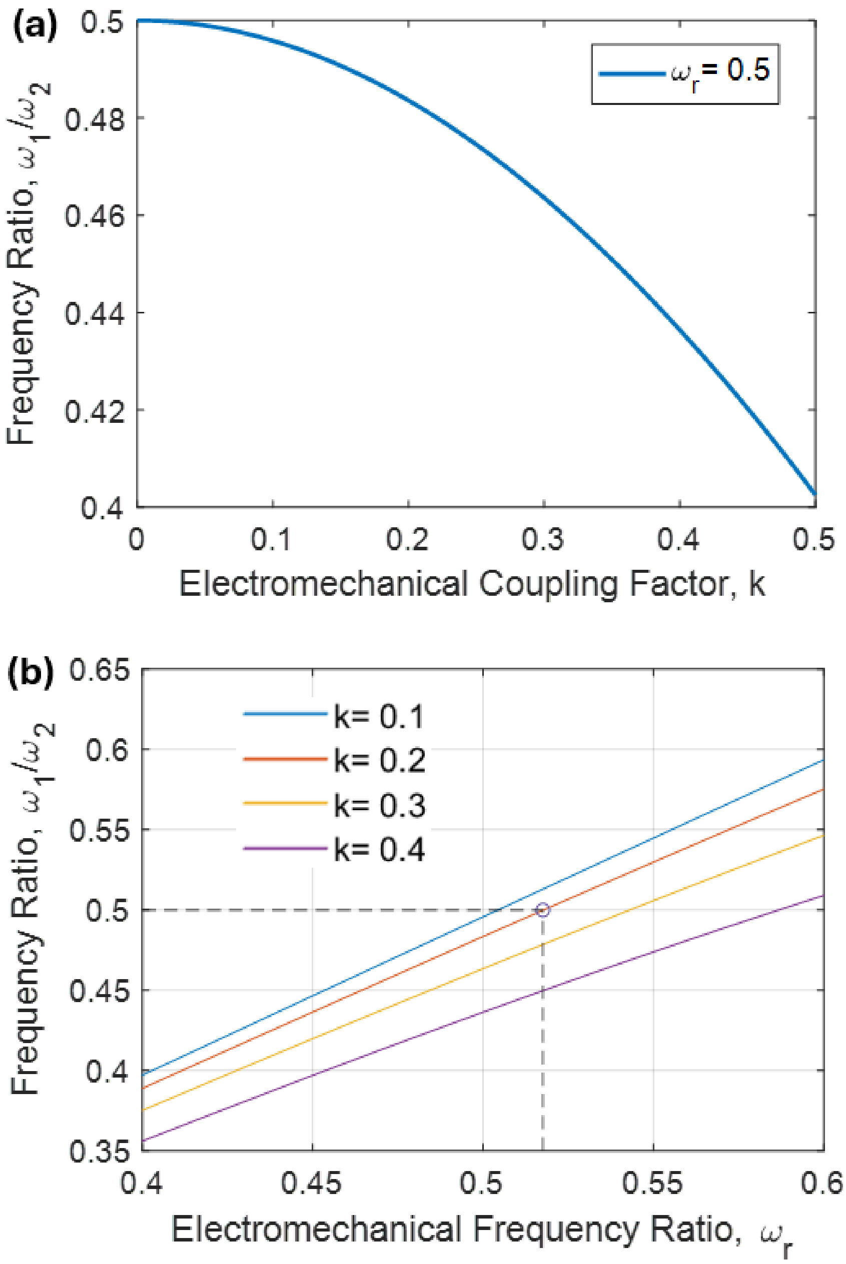

Figure 15: a) the response of the frequency ratio with increasing the EMCF while having the electromechanical frequency ratio as 0.5. b) the detuning between the frequency ratio and the electromechanical frequency ratio with increasing the EMCF.

The effect of the internal resonance from the nonlinear capacitor starts to appear by creating an energy transfer between the modes. Before τ=522, the structure is under oscillation and the piezoelectric patch starts to deform to feed the electrical circuit with constant electrical charges. After τ=522, the energy exchange between the modes can be observed by damping the amplitude of the structure and transferring more energy to the circuit. After τ=1038, both modes reach steady states, and the vibration of the structure is mitigated because the same energy exchange rate remains constant through time. Although it may seem that the dimensionless time (τ) required for the system to achieve a steady state is large, it is considered acceptable since the physical time required to achieve this state is 13.4 seconds.

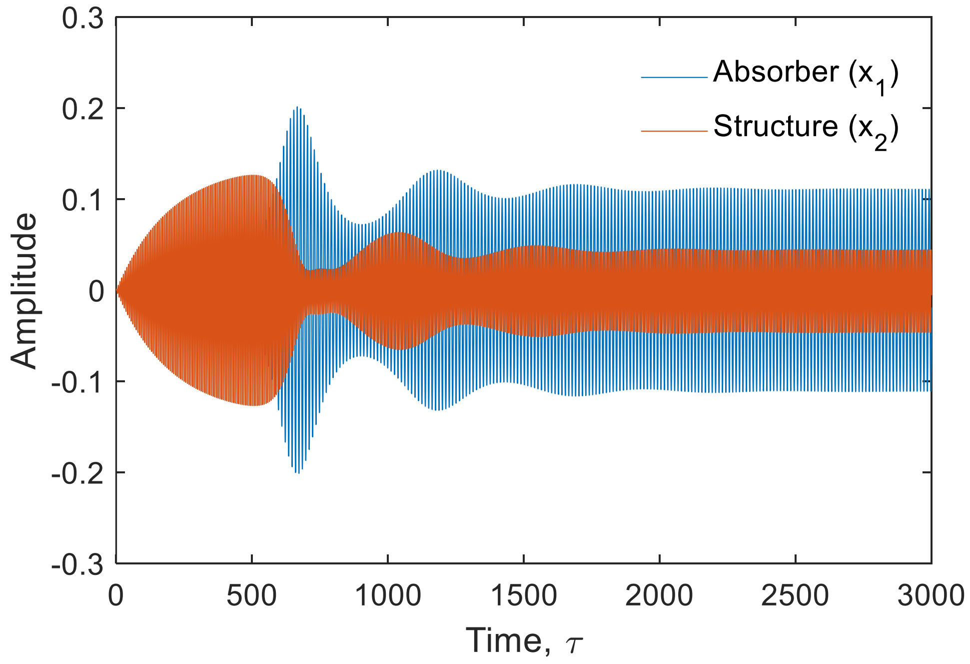

Figure 16: The time response for the electrical mode (Circuit) and the mechanical mode (Structure).

The primary goal of inducing the internal resonance in any system is to produce a saturation phenomenon, in which, regardless of the amount of excitation applied to the structure, the energy transferred to the mechanical mode will remain constant after a certain amount of excitation and create a threshold. The saturation phenomena could not be observed in the time response simulations, it requires a force response as the one that is presented in Figure 17. The figure shows how the mechanical amplitude follows a linear behavior as usual, increasing excitation while the circuit is inactive. However, after exceeding a threshold excitation of 0.16 N, the energy transfer occurs and the saturation phenomenon appears by creating a threshold of 0.044 for the mechanical amplitude (structure), while all the excessive energy is directly transferred to the unexcited electrical mode (circuit) and activates it. The saturation amplitude and the forcing threshold depend on the circuit's resistance and capacitance of the circuit, the modal damping of the structure, and the piezoelectric patch size and configuration. The significance of those characteristics will be further investigated in the upcoming sections.

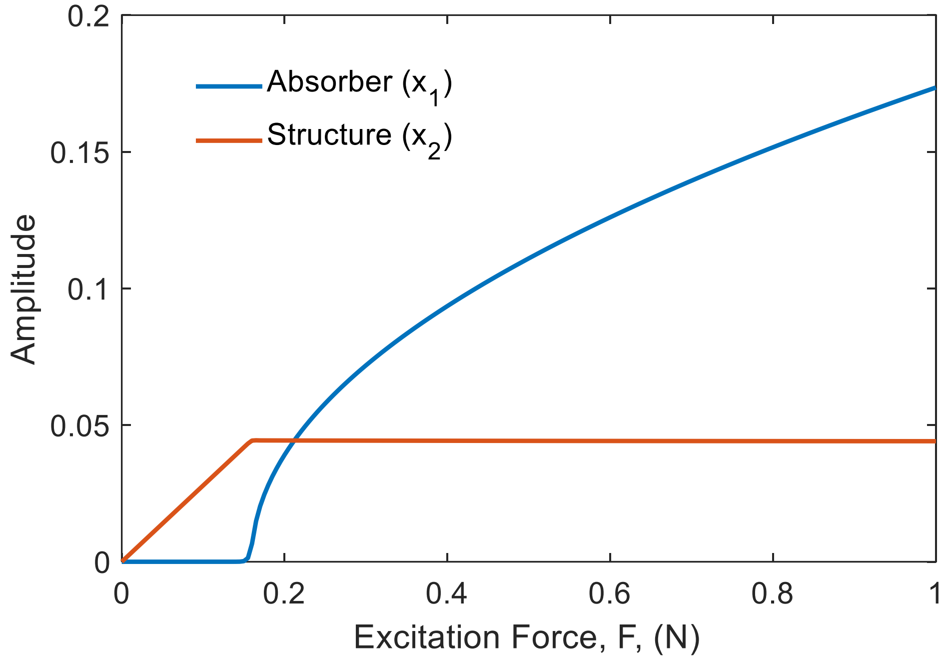

Figure 17: The force response for the electrical mode (Circuit) and the mechanical mode (Structure).

To demonstrate the model's performance, Figure 18 presents a comparison of the response for a cantilever beam under two different conditions: in the first scenario, the beam vibrates while uncoupled from the shunted circuit when subjected to harmonic excitation. In contrast, the second scenario links the beam to a shunted circuit (coupled), subjecting it to the same excitation as in the first case. This figure illustrates how crucial and efficient the absorber is. Figure 18a presents the time response for both cases under an excitation force of 0.5 N. We observe a significant gap in the structure amplitude value between the two cases, demonstrating the shunted circuit's excellent performance in damping the structure's vibration. This can also be seen in Figure 18b, where the uncoupled beam amplitude will increase linearly with the increasing excitation force, unlike the coupled case, where after exceeding the forcing threshold (0.16 N), the amplitude will remain constant at (0.044), therefore exploiting the saturation phenomenon to the fullest.

4.3. Design Parameters

To perform a parametric study on the system for optimizing the parameters to have the best performance, we are going to divide the parameters into three categories: the parameters that are circuit-related, the second is for the modal damping which is structural-related, and the last is for parameters that are patch-related.

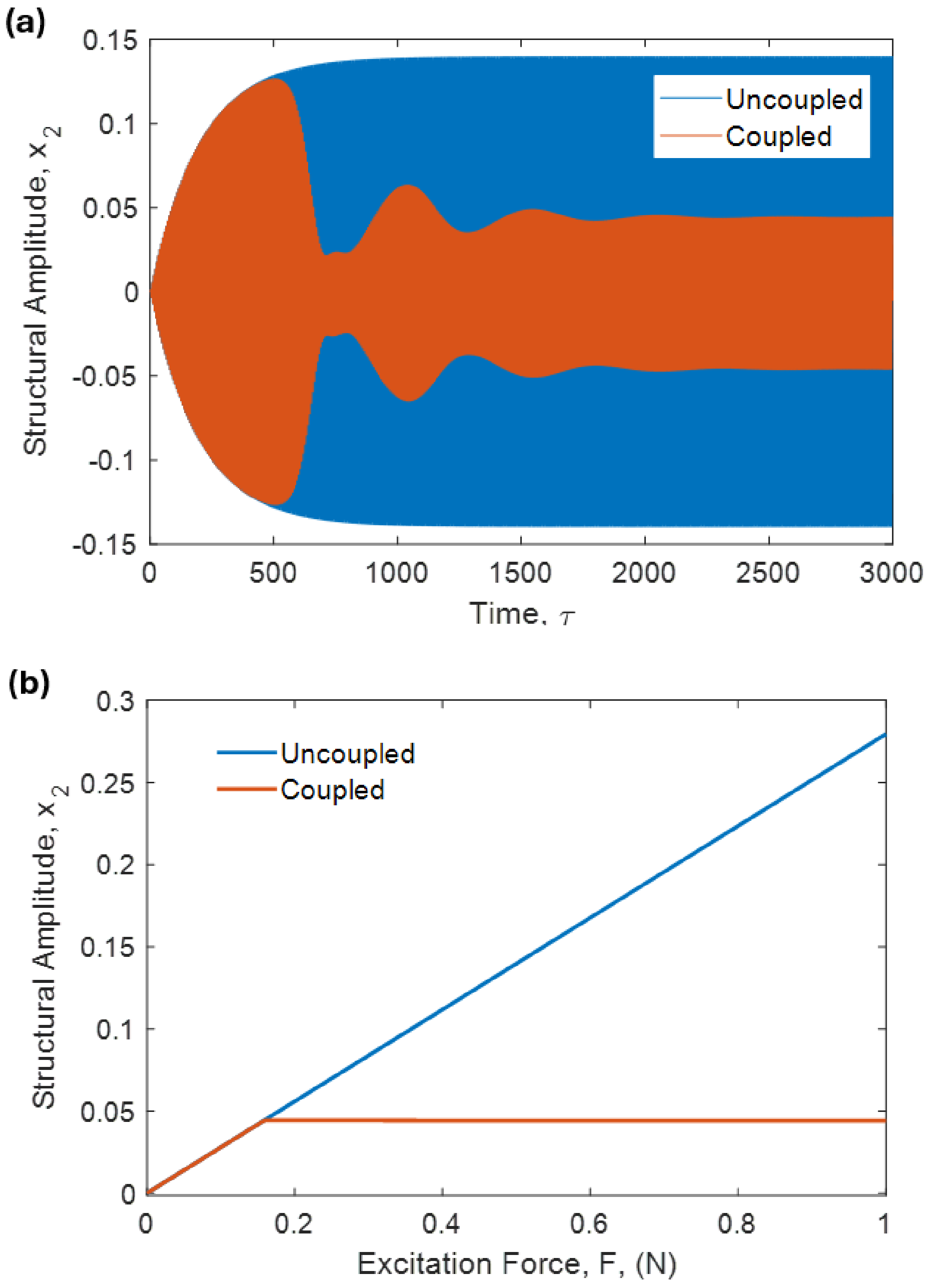

Figure 18: a) the time response for the cantilever beam while it's coupled and uncoupled to the shunted circuit and under excitation of 0.5 N. b) the force response for the cantilever beam while it's coupled and uncoupled to the shunted circuit.

4.3.1. Circuit Parameters

We first investigate the effect of the design parameters by studying the system's behavior under various electrical damping values in the shunted circuit, which the electrical resistance controls. We confirmed this by monitoring the force response for the mechanical structure across four different resistors in the circuit as shown in Figure 19**.** A cantilever beam connected to a circuit with a resistor of 4000 Ω has a forcing threshold and a saturation limit equal to 0.18 N and 0.05, respectively, while on the other hand, a 3000 Ω has a forcing threshold of 0.145 N and a saturation limit of 0.04. This indicates that with decreasing resistance (decreasing electrical damping), the saturation limit and the forcing threshold will decrease, thus enhancing the circuit performance. The results in Figure 19 are the same as those in [50] where an RL piezoelectric shunted circuit showed that a smaller resistor gives better damping to the structure.

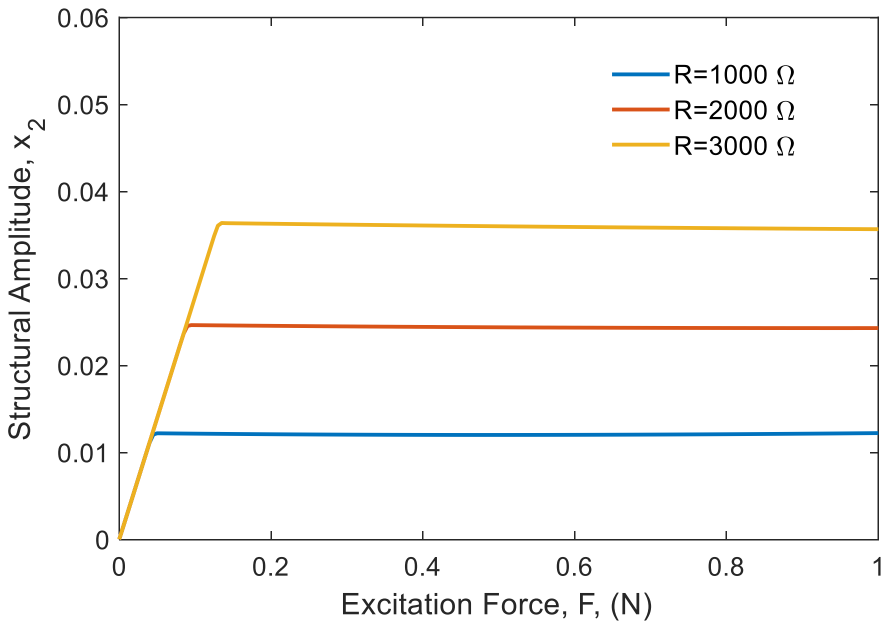

Figure 19: The force response for the mechanical mode (Structure) for different electrical resistor values in the shunted circuit.

The nonlinear constant (N) is another design parameter that can influence both the saturation amplitude and the forcing threshold. This parameter's role is to act as a constant gain for controlling the significance of the quadratic nonlinearity in the system. We examined the effect of the nonlinear constant on the absorber's performance by simulating three cases, each with the same resistor and inductor, but with different nonlinear constant values for the nonlinear capacitor ($1 \times 10^{10}\ V/C^2,\ 2 \times 10^{10}\ V/C^2, and\ 3 \times 10^{10}\ V/C^2$). The absorber generates internal resonance in all three cases, presenting the saturation phenomenon in each case. However, Figure 20 displays an inverse proportional relationship between the nonlinear constant and the saturation amplitude; increasing the nonlinear constant will decrease the amplitude, Eq. (55) and Eq. (56) confirm this, as an increase in the nonlinear constant magnifies the nonlinear coupling terms in the system, increasing the coupling between the structure and the absorber and therefore enhancing the vibration damping of the structure.

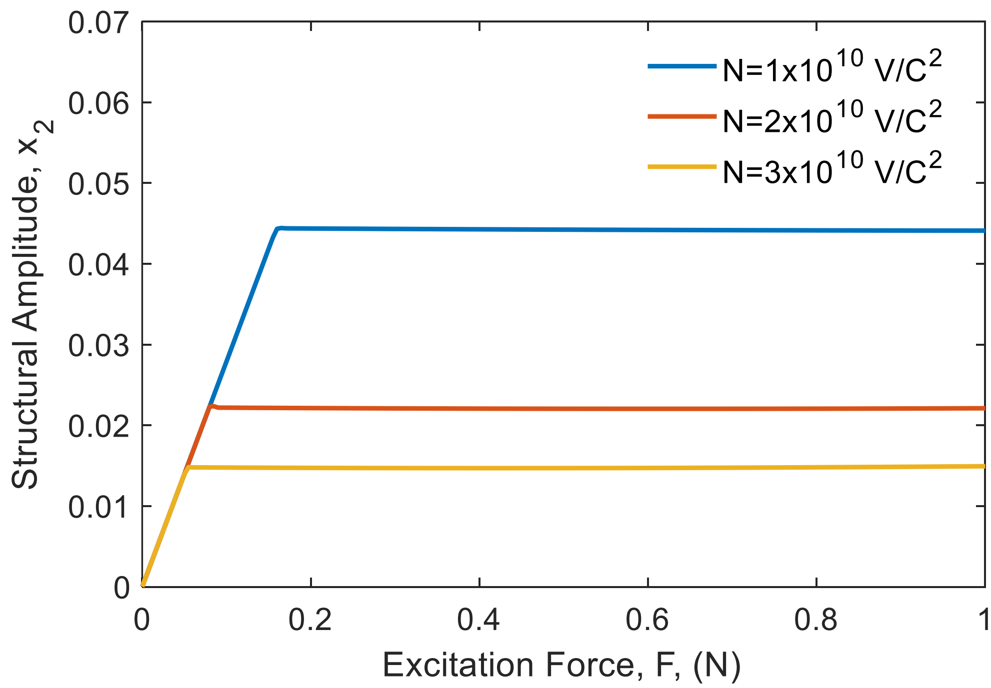

Figure 20: The force response for the mechanical mode (Structure) for different nonlinear constant values for the nonlinear capacitor.

4.3.2. Structure Parameters (modal damping ratio)

As we can see in the previous results, the performance of the shunted circuit can significantly depend on the electrical element's value. In addition, other factors affect energy exchange between the structure and absorber. The structure's modal damping ratio plays a significant role in the emergence of the saturation phenomenon. Figure 21 shows how the damping ratio variation can affect the amount of excitation needed to activate the energy transfer (forcing threshold).

Unlike the electrical components of the circuit, changing the structure's damping ratio does not affect the saturation amplitude. The saturation amplitude is the same for the three different values of damping ratios (0.044). However, the forcing threshold varies in each case. Increasing the modal damping ratio will increase the forcing threshold.

On the other hand, as we reduce the modal damping, the forcing threshold decreases, ensuring that the system damps the vibration at earlier stages of force.

However, this may impact the system's behavior, resulting in some underdamped-like behavior for the damping ratio of 0.003. This may not seem to be a problem because this small disturbance is acceptable, but for much smaller damping ratios, this behavior can turn into a severe disturbance that can vanish the saturation phenomena

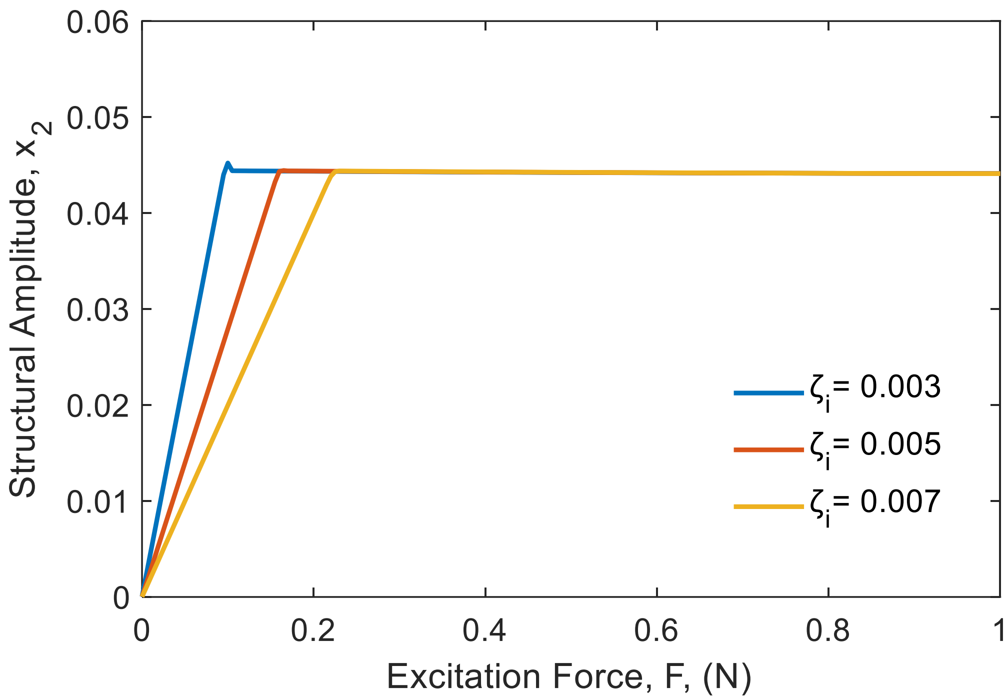

Figure 21: The force response for the mechanical mode (Structure) for a variation of modal damping ratios of the cantilever beam.

4.3.3. Piezoelectric Patch Parameters

The piezoelectric patch, due to its unique electromechanical coupling properties, is the system's core and the link between the structure and the circuit. Therefore, optimizing the patch's characteristics is crucial for achieving a high electromechanical coupling factor and improved performance. Numerous factors, including the placement of the piezoelectric patch, influence the rate of energy conversion a piezoelectric patch can handle, as demonstrated by the calculation of the electromechanical coupling coefficient. We will place the piezoelectric patch in three different locations on top of the cantilever beam, as illustrated in Figure 22.

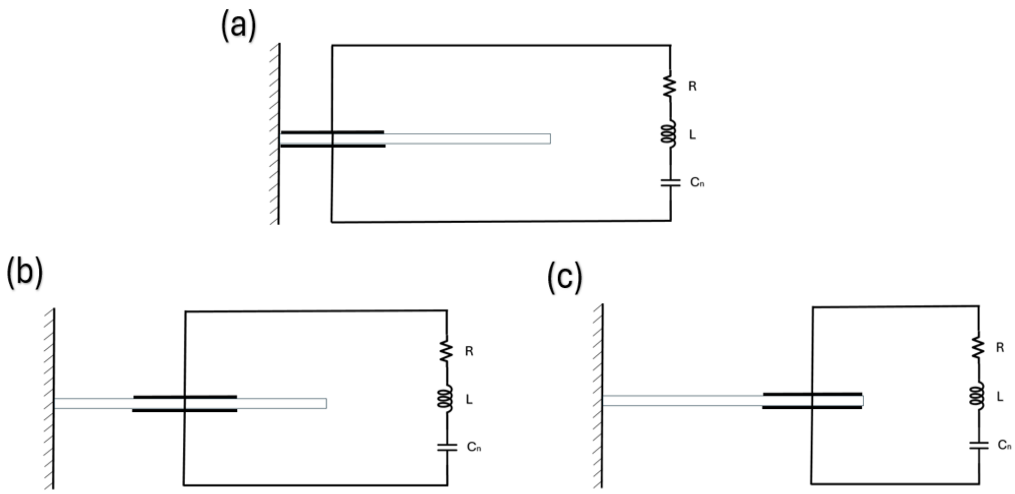

Figure 22: The piezoelectric patch position on the cantilever beam: a) on the fixed end, b) on the center, and c) on the free end.

The first location is on the beginning of the fixed side ($k_1 = 6.31\%$), then at the center ($k_1 = 2.97\%$), and finally on the tip of the beam ($k_1 = 0.06\%$) and because of the variation in the EM coupling factor, each frequency ratio is tuned based on Figure 15 to achieve a 2:1 frequency ratio. In Figure 23**,** we can see that there is a big difference between how well the patch works in the three places. The numerical simulation showed that the place with the highest EMCF (Position (a)) does the best out of all the places based on both their saturation amplitude and their forcing threshold values. A justification and explanation for this can be found in [51], where they found out that the most stored strain energy is on the fixed side of the beam, leading to a higher rate of energy conversion and a higher EMCF. Position (b) didn't mitigate the vibration in the same efficient way that Position (a) did, but it was still considered a satisfactory performance. However, due to its low EMCF, Position (c) performed significantly worse than the other two positions with a 76% increase in saturation amplitude compared to Position (b).

The size of the piezoelectric patch can significantly affect the performance of the shunted circuit. Two characteristics, the EMCF and the capacitance of the patch, demonstrate the crucial role the patch size plays in the system's performance. To analyze the patch size effect, we are going to study the two main factors that matter in the dimensions of the piezoelectric patch, which are the surface area and the thickness of the patch. The performance of four patches with different lengths and widths is going to be tested next to the original patch (Patch A) that was chosen in the previous results for the surface area. Table 1 provides the dimensions of the patches.

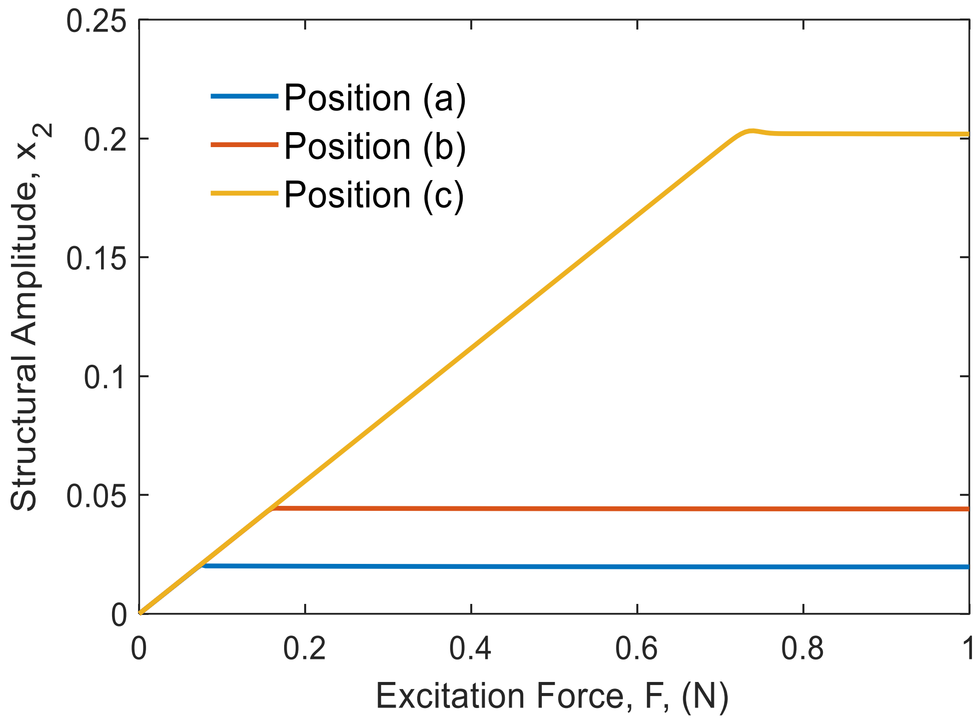

Figure 23: The force response for the mechanical mode (structure) for three patch positions (on the fixed end, on the center, on the free tip).

Figure 24 presents the variation of structural amplitudes from the piezoelectric patches based on each patch's dimensions and the resulting electromechanical coupling factor. The figure combines the results for five different patches. We selected the first patch (Patch A) as the reference patch for this study and compared it with the other patches. The second and third patches (Patch B and Patch C) are the smallest and largest patches, respectively, in terms of surface area, electromechanical coupling factor, and capacitance. Figure 24 reveals a significant difference, suggesting that a larger patch can yield superior performance, and vice versa.

Table 1: A size variation and properties for five different piezoelectric patches.

Patch	**Dimensions (L_p x b_p)**	**Surface area**	**EMFC (k_1)**	**PZT Capacitance**
A	0.10 m x 0.015 m	0.0015 m^2	2.97 %	96.58 nF
B	0.09 m x 0.014 m	0.00126 m^2	2.71%	81.13 nF

C	0.11 m x 0.016 m	0.00176 m^2	3.23%	113.3 nF
D	0.12 m x 0.01167 m	0.0014 m^2	2.90%	90.17 nF
E	0.08 m x 0.0175 m	0.0014 m^2	2.85%	90.14 nF

Moreover, to understand the method of optimizing the patch size, we studied two patches (Patch D and Patch E) that have the same surface area but different dimensions. The first patch (Patch D) has a higher length-to-width ratio than the other patch (Patch E). This caused (Patch D) to have better capacitance and higher EMCF, as well as better suppression than (Patch E), indicating that the absorber efficiency is a little bit more sensitive to the length of the patch than its width.

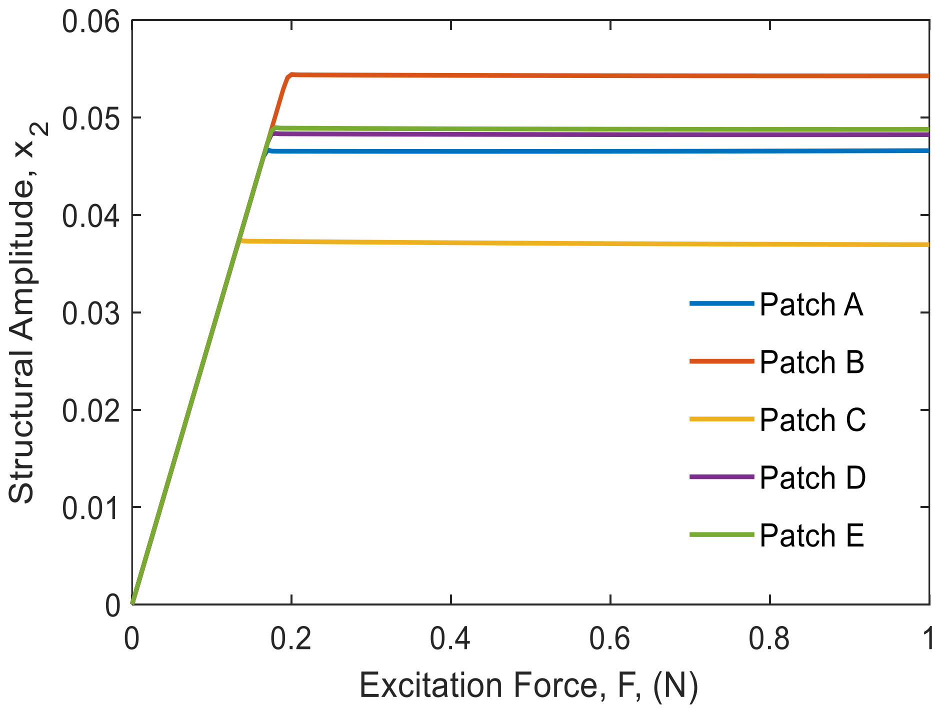

Figure 24: The force response for the mechanical mode (structure) for five piezoelectric patches that have different surface areas.

Another factor that should be considered in studying the patch size effect is the thickness of the patch. As we saw in the previous study, increasing the patch surface area will increase the EMCF and the capacitance, but unfortunately, we can’t determine who has the bigger effect on the performance of the absorber. Therefore, varying the patch thickness as shown in Table 2 will be a good approach for exploring the effect of varying the EMCF and the capacitance, with one increasing while the other decreasing.

Table 2: A thickness variation and properties for three different piezoelectric patches.

Patch	**Thickness (t_p)**	**Electromechanical factor (k_1)**	**PZT Capacitance**
A	0.3 mm	2.00 %	161.0 nF
B	0.5 mm	2.97 %	96.58 nF
C	0.7 mm	3.98%	68.98 nF

Figure 25 charts the force responses of three distinct patches. The first plot (Patch A) showed a larger saturation amplitude and forcing threshold compared to the other patches. As we increase the thickness from the second plot (Patch B) to the third plot (Patch C), the EMCF increases while the capacitance continues to decrease. This indicates that the EMCF is the most crucial factor in piezoelectric patch design and should be considered as the objective function when aiming to optimize the patch size.

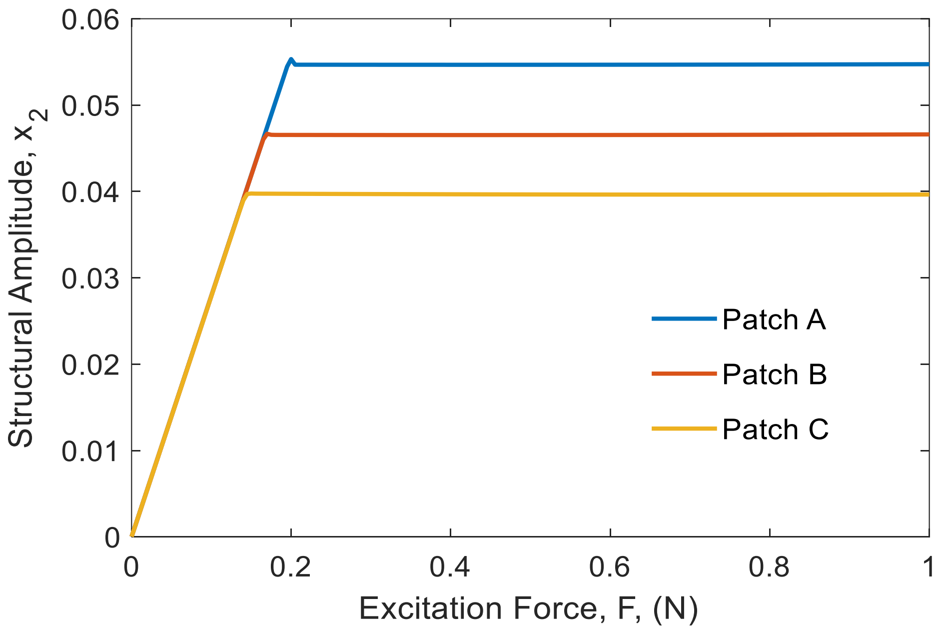

Figure 25: The force response for the mechanical mode (structure) for three piezoelectric patches that have different thicknesses.

4.4. Response of the Nonlinear Structure Coupled with the Shunted Circuit

Following the previous section's study, we first investigate the nonlinear cantilever beam's behavior without connecting the piezoelectric shunted circuit to the structure. This will help demonstrate how the structure's behavior becomes amplitude-dependent upon the frequency. Figure 26 illustrates the frequency response as the force excitation amplitude increases on a cantilever beam that shares the same dimensions and properties selected in the linear section. The figure highlights a significant distinction between a linear structure and a nonlinear structure: the nonlinear structure experiences amplitude shifting due to the hardening effect, which intensifies as the excitation force increases. The first section of the figure illustrates how the nonlinear structure responds to an applied force of 0.1 N. It shows almost a linear response because the amplitude is low and can't cause the nonlinear effect yet. As we increase the excitation to 0.3 N, the structure's amplitude bends to the right, signifying the existence of a multivalued frequency region that triggers a jump phenomenon. This hardening stems from the geometrical cubic nonlinear term in Eq. (63). Because we are only interested in the first mode, the only nonlinear effect that appears is the hardening effect, in the case of the second and third modes, the dominant term is the inertia term that induces a softening

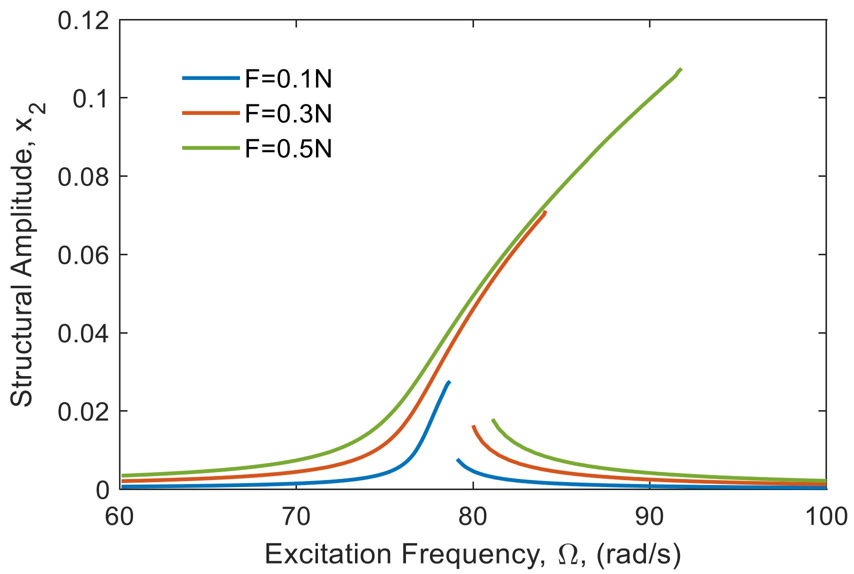

Figure 26: The frequency response for a nonlinear cantilever beam under different excitations.

effect [52]. Increasing the excitation force to 0.5 N yields a higher amplitude and more bending in the curve with the same trend. Many applications do not favor this behavior as it can lead to catastrophic failure in the structure.

Figure 27 displays the frequency response of the nonlinear structure mode for two situations: first when the structure is not connected to the absorber as in Figure 26, and second, when it is coupled to the shunted circuit. This shows how well the shunted circuit works to stop the vibration of a nonlinear structure. In the coupled cases, we tune the shunted circuit to half the natural frequency of the structure to create the saturation phenomenon. The absorber parameters are going to be optimized based on the parametric analysis in the last section to obtain the optimal performance. The patch will be attached to the fixed tip of the beam, also, the non-linear constant for the non-linear capacitor (N) will be chosen as $3 \times 10^{10}\ V/C^2$.

When the cantilever beam vibrates under an excitation force of 0.1 N, Figure 27a shows how the absorber can damp it. A double peak phenomenon is visible, confirming the excellent performance of the shunted circuit. However, this does not demonstrate the absorber's ability to mitigate nonlinear structures, as the excitation force alone is insufficient to induce a significant nonlinear behavior in the structure. Therefore, the structure vibrates as if it were a linear structure.

To excite the nonlinear behavior**,** Figure 27b demonstrates the significant impact of nonlinearity in shifting the amplitude peak to the right after increasing the force to 0.3 N. In the coupled case, we see a significant reduction in amplitude. Increasing the excitation force to 0.5 N, as shown in Figure 27c, shows an increase in the amplitude with more amplitude peak shifting. The coupled case demonstrates that even with higher excitations and amplitudes, the absorber keeps damping the vibration to a relatively small amplitude, indicating its great performance.

Adding on the previous results, Figure 28a presents the time response for the nonlinear beam under excitation of 0.5 N. The energy transfer from the structure and the damping of it can be seen after $\tau = 100$ (1.3 seconds). It can be observed that the absorber in the coupled case takes a time of $\tau = 290$ (3.76 seconds) to reach a steady state and dampen the vibration. Also in Figure 28b**,** we can see the force response of the nonlinear structure and how with increasing the force the hardening nonlinear effect starts to appear in the Uncoupled case, However, when coupling the structure to the shunted circuit, the internal resonance is activated and the saturation limit appears after excitation of 0.035 N.

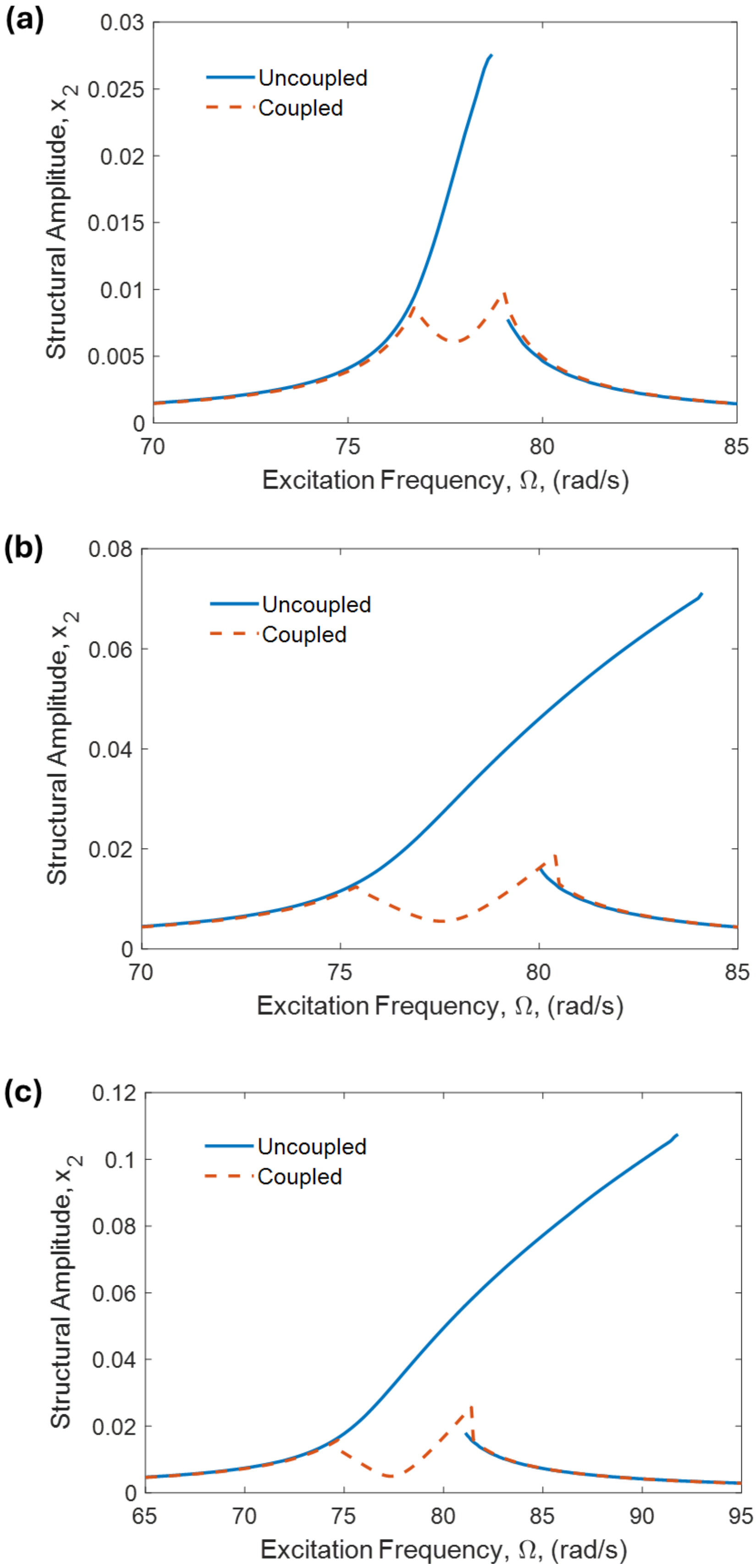

Figure 27: The frequency response for nonlinear cantilever beam in two cases: coupled to a shunted circuit and uncoupled under excitation of a) 0.1 N, b) 0.3 N, c) 0.5 N.

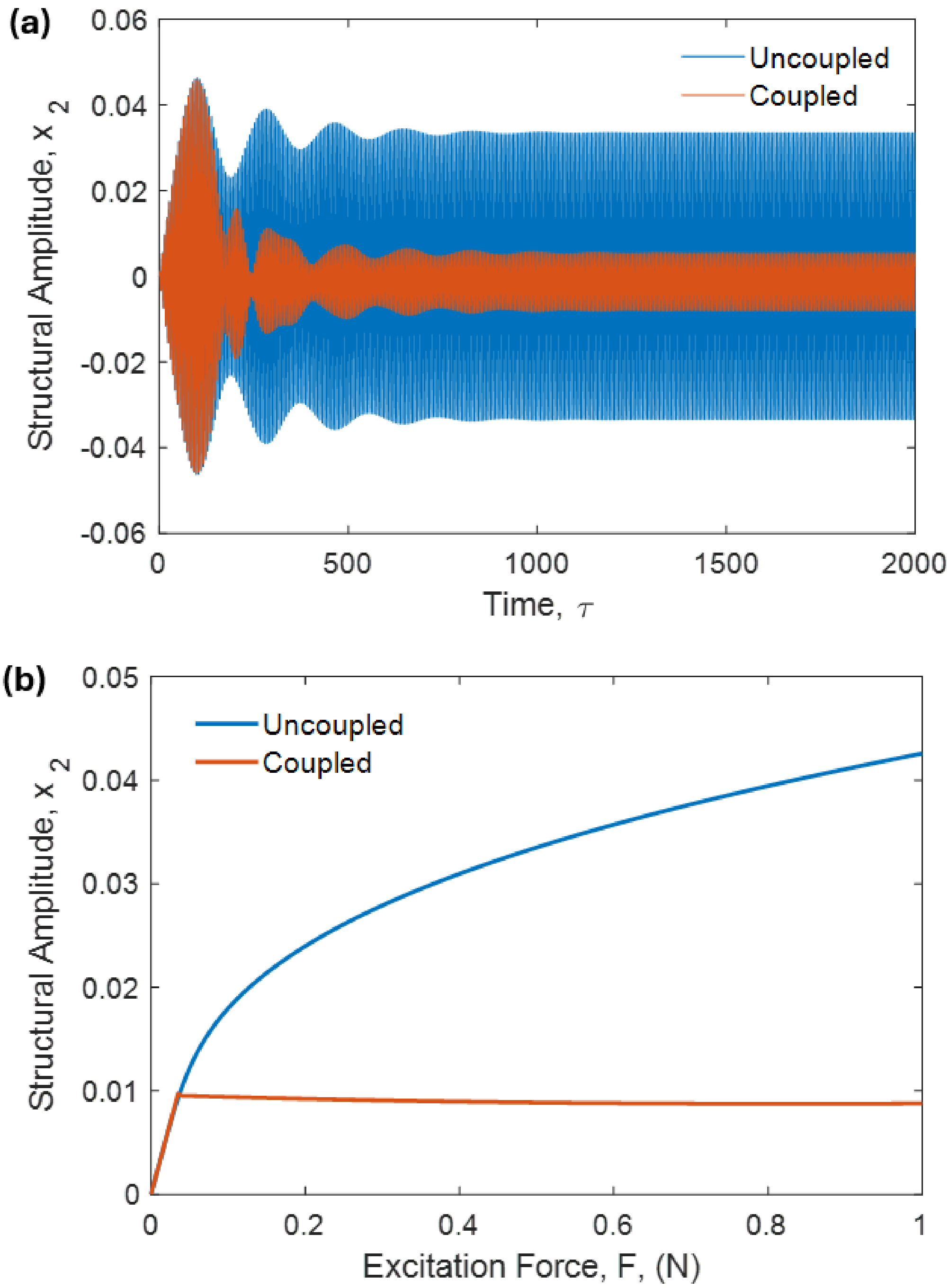

Figure 28: a) the time response for the nonlinear structure while it is coupled and uncoupled under an excitation of 0.5 N b) the force response for the nonlinear structure while it is coupled and uncoupled.

Chapter 5. Conclusion and Future Work

In this thesis, piezoelectric shunted circuits are considered to mitigate the vibration of a cantilever beam. The nonlinear absorber consists of a piezoelectric patch and a shunted circuit. The shunted circuit is considered a semi-active control system. This work aims to create an internal resonance phenomenon by adding a nonlinear electrical component into the shunted circuit and creating a quadratic nonlinear coupling between the modes of the structure (cantilever beam) and the absorber (circuit) while having the frequency ratio between them to be 2:1 respectively. Also, the performance of the absorber was investigated when damping a nonlinear structure to study how the absorber behaves when countering another source of nonlinearity.

A mathematical model was developed to numerically simulate the damping performance of the nonlinear absorber when coupled to a linear structure, the absorber demonstrated a great performance, especially with creating a saturation limit for the structure where with increasing the excitation force, the amplitude of structural mode remains constant. A parametric analysis was performed to serve as a design guideline for optimizing the system parameters, we concluded that increasing the modal damping ratio and the constant of the nonlinear capacitor while decreasing the resistor value will enhance the suppression from the absorber. Also, the piezoelectric patch position and size were studied, and the results proved that the most optimum location for a patch to be placed on is the fixed end of the beam due to the higher strain energy that is stored there.

A cantilever beam with cubic geometrical nonlinearity was presented to study the performance of the shunted circuit while dealing with an external source of nonlinearity. The results demonstrated the ability of the shunted circuit by showing the frequency response for the structure under different levels of excitation and maintaining a saturation limit for the structural mode amplitude in the force response.

The current work might be expanded to investigate more complicated scenarios, since it successfully modelled an absorber that can dampen a single mode of vibration in a structure that exhibits geometrical nonlinearity. Researchers may look at the possibility of dampening several vibration modes by using various circuit designs. Furthermore, there is plenty of room to experiment with other forms of electrical nonlinear components. These might be constructed to successfully reduce vibrations in structures with a wider range of nonlinearities, increasing the adaptability and usability of vibration damping systems in a variety of structural designs. Moreover, experimental validation of this study is required to test the mathematical models and simulations, provide practical insights, and prove the efficiency of the suggested methodologies in real-world applications.

References

[1] E. A. Al-Bahkali, H. Elkenani and M. Souli, "Failure and fatigue life due to random vibration in aircraft applications," Multiphysics Simulations in Automotive and Aerospace Applications. Academic Press, 131-154. 2021.

[2] H. A. Sodano, D. J. Inman and G. Park, "A review of power harvesting from vibration using piezoelectric materials," Shock and Vibration Digest, vol. 36, (3), 197–206. 2004.

[3] R. L. Forward, "Electronic damping of vibrations in optical structures," Applied Optics, vol. 18, (5), 690–697, 1979.

[4] D. Niederberger and M. Morari, "An autonomous shunt circuit for vibration damping," Smart Materials and Structures, vol. 15, (2), pp. 359, 2006.

[5] D. D. L. Chung, " Materials for vibration damping." Journal of Materials Science, vol. 36, (24), pp. 5733–5737, 2001.

[6] H. Ji, J. Qiu, Y. Wu, C. Zhang, "Semi-active vibration control based on synchronously switched piezoelectric actuators," International Journal of Applied Electromagnetics and Mechanics, vol. 59, pp. 299–307, 2019.

[7] A. Baz, "Active and Passive Vibration Damping," John Wiley & Sons, pp. 1–10, 2018.

[8] F. Mangussi and D. H. Zanette, "Internal resonance in a vibrating beam: a zoo of nonlinear resonance peaks," PloS One, vol. 11, (9), pp. e0162365, 2016.

[9] A. H. Nayfeh, D. T. Mook and L. R. Marshall, "Nonlinear coupling of pitch and roll modes in ship motions," Journal of Hydronautics, vol. 7, (4), pp. 145–152, 1973.

[10] J. C. Ji, "Design of a nonlinear vibration absorber using three-to-one internal resonances," Mechanical Systems and Signal Processing, vol. 42, (1), pp. 236–246, 2014.

[11] N. W. Hagood and A. von Flotow, "Damping of structural vibrations with piezoelectric materials and passive electrical networks," Journal of Sound and Vibration, vol. 146, (2), pp. 243–268, 1991.

[12] S. Wu, "Piezoelectric shunts with a parallel RL circuit for structural damping and vibration control," Smart Structures and Materials 1996: Passive Damping and Isolation, vol. 2720, pp. 259-269, 1996.

[13] K. Yamada, "Complete passive vibration suppression using multi-layered piezoelectric element, inductor, and resistor," Journal of Sound and Vibration, vol. 387, pp. 16–35, 2017.

[14] B. Lossouarn, M. Aucejo, J&F. Deü, B. Multon, "Design of inductors with high inductance values for resonant piezoelectric damping," Sensors and Actuators A: Physical, vol. 259, pp. 68–76, 2017.

[15] J. J. Hollkamp, "Multimodal passive vibration suppression with piezoelectric materials and resonant shunts," Journal of intelligent material systems and structures, vol. 5, (1), pp. 49–57, 1994.

[16] S. Wu, "Method for multiple mode piezoelectric shunting with single PZT transducer for vibration control," Journal of intelligent material systems and structures, vol. 9, (12), pp. 991–998, 1998.

[17] S. Wu, "Method for multiple-mode shunt damping of structural vibration using a single PZT transducer," Smart Structures and Materials 1998: Passive Damping and Isolation, vol. 3327, pp. 159-168, 1998.

[18] S. Behrens and S. R. Moheimani, "Current flowing multiple-mode piezoelectric shunt dampener," Smart Structures and Materials 2002: Damping and Isolation, vol. 4697, pp. 217-226, 2002.

[19] S. Behrens, S. R. Moheimani and A. J. Fleming, "Multiple mode current flowing passive piezoelectric shunt controller," Journal of Sound and Vibration, vol. 266, (5), pp. 929–942, 2003.

[20] J. Gripp and D. A. Rade, "Vibration and noise control using shunted piezoelectric transducers: A review," Mechanical Systems and Signal Processing, vol. 112, pp. 359–383, 2018.

[21] G. Raze et al, "Multimodal vibration damping using a simplified current blocking shunt circuit," Journal of intelligent material systems and structures, vol. 31, (14), pp. 1731–1747, 2020.

[22] J. Jeon, "Passive vibration damping enhancement of piezoelectric shunt damping system using optimization approach," Journal of Mechanical Science and Technology, vol. 23, pp. 1435–1445, 2009.

[23] J. Jeon, "Passive acoustic radiation control for a vibrating panel with piezoelectric shunt damping circuit using particle swarm optimization algorithm," Journal of Mechanical Science and Technology, vol. 23, pp. 1446–1455, 2009.

[24] A. N. Wahid, A. G. Muthalif and K. A. Nor, "Investigating negative capacitance shunt circuit for broadband vibration damping and utilizing ACO for optimization," Int.J.Circuits Electron, vol. 1, pp. 168–173, 2016.

[25] G. Caruso, "A critical analysis of electric shunt circuits employed in piezoelectric passive vibration damping," Smart Materials and Structures, vol. 10, (5), pp. 1059, 2001.

[26] P. Soltani et al, "Piezoelectric vibration damping using resonant shunt circuits: an exact solution," Smart Materials and Structures, vol. 23, (12), pp. 125014, 2014.

[27] T. Bailey and J. E. Hubbard Jr, "Distributed piezoelectric-polymer active vibration control of a cantilever beam," Journal of Guidance, Control, and Dynamics, vol. 8, (5), pp. 605–611, 1985.

[28] J. J. Dosch, D. J. Inman and E. Garcia, "A self-sensing piezoelectric actuator for collocated control," Journal of intelligent material systems and structures, vol. 3, (1), pp. 166–185, 1992.

[29] E. Anderson, N. Hagood and J. Goodliffe, "Self-sensing piezoelectric actuation-analysis and application to controlled structures," 33rd Structures, Structural Dynamics and Materials Conference, pp. 125014, 1992.

[30] R. L. Forward, " Electromechanical Transducer-Coupled Mechanical Structure with Negative Capacitance Compensation Circuit," U.S. Patent No. 4,158,787 ,1979.

[31] B. De Marneffe and A. Preumont, "Vibration damping with negative capacitance shunts: theory and experiment," Smart Materials and Structures, vol. 17, (3), pp. 035015, 2008.

[32] S. Behrens, A. J. Fleming and S. Moheimani, "A broadband controller for shunt piezoelectric damping of structural vibration," Smart Materials and Structures, vol. 12, (1), pp. 18, 2003.

[33] C. H. Park and H. C. Park, "Multiple-mode structural vibration control using negative capacitive shunt damping," KSME International Journal, vol. 17, pp. 1650–1658, 2003.

[34] B. S. Beck, K. A. Cunefare, M. Collet, M. Ruzzene, "Active vibration control of a stiffened panel through application of negative capacitance shunts," Active and Passive Smart Structures and Integrated Systems 2011, vol.7977, pp. 121–132, 2011.

[35] O. Heuss, R. Salloum, D. Mayer, And T. Melz, "Tuning of a vibration absorber with shunted piezoelectric transducers," Archive of Applied Mechanics, vol. 86, pp. 1715–1732, 2016.

[36] W. W. Clark, "Vibration control with state-switched piezoelectric materials," Journal of intelligent material systems and structures, vol. 11, (4), pp. 263–271, 2000.

[37] C. Richard, D. Guyomar, D. Audigier, H. Bassaler, "Enhanced semi-passive damping using continuous switching of a piezoelectric device on an inductor," Smart Structures and Materials 2000: Damping and Isolation, vol. 3989, pp. 288-299 ,2000.

[38] E. Lefeuvre, A. Badel, L. Petit, C. Richard, and D. Guyomar, "Semi-passive piezoelectric structural damping by synchronized switching on voltage sources," Journal of intelligent material systems and structures, vol. 17, (8-9), pp. 653–660, 2006.

[39] L. R. Corr and W. W. Clark, "A novel semi-active multi-modal vibration control law for a piezoceramic actuator," J.Vib.Acoust., vol. 125, (2), pp. 214–222, 2003.

[40] W. Tang, L. B. Wang, Y. M. Ren, B. Bao, and J. J. Cao, "Design and experimental analysis of self-sensing SSDNC technique for semi-active vibration control," Smart Materials and Structures, vol. 27, (8), pp. 085028, 2018.

[41] R. S. Haxton and A. D. S. Barr, "The autoparametric vibration absorber," 1972.

[42] M. Sayed and M. Kamel, "1:2 and 1:3 internal resonance active absorber for non-linear vibrating system," Applied Mathematical Modelling, vol. 36, (1), pp. 310–332, 2012.

[43] S. El-Serafi, M. Eissa and T. El-Ghareeb, "1: 4 Internal resonance active absorber for non-linear vibrating system," Int.J.Pure Appl.Math, vol. 28, (1), pp. 515–537, 2006.

[44] S. S. Oueini, A. H. Nayfeh and J. R. Pratt, "A nonlinear vibration absorber for flexible structures," Nonlinear Dynamics., vol. 15, pp. 259–282, 1998.

[45] Z. A. Shami, C. Giraud-Audine and O. Thomas, "A nonlinear piezoelectric shunt absorber with a 2: 1 internal resonance: theory," Mechanical Systems and Signal Processing, vol. 170, pp. 108768, 2022.

[46] O. Thomas, J. Deü and J. Ducarne, "Vibrations of an elastic structure with shunted piezoelectric patches: efficient finite element formulation and electromechanical coupling coefficients," International journal for numerical methods in engineering, vol. 80, (2), pp. 235–268, 2009.

[47] H. N. Arafat, A. H. Nayfeh and C. Chin, "Nonlinear nonplanar dynamics of parametrically excited cantilever beams," Nonlinear Dyn., vol. 15, pp. 31–61, 1998.

[48] The material characteristics of piezoceramics., Fuji Ceramics Corporation, 2022. http://www.fujicera.co.jp/product/e/01/mat.table_e.pdf.

[49] B. Götz, R. Platz and T. Melz, "Effect of uncertain boundary conditions and uncertain axial loading on lateral vibration attenuation of a beam with shunted piezoelectric transducers," Proceedings of ISMA2014 Including USD2014 International Conference on Uncertainty in Structural Dynamics, 2014.

[50] C. H. Park, "Dynamics modelling of beams with shunted piezoelectric elements," Journal of Sound and Vibration., vol. 268, (1), pp. 115–129, 2003.

[51] A. Erturk, P. A. Tarazaga, J. R. Farmer, and d. J. Inman "Effect of strain nodes and electrode configuration on piezoelectric energy harvesting from cantilevered beams," 2009.

[52] P. F. Pai and A. H. Nayfeh, "Non-linear non-planar oscillations of a cantilever beam under lateral base excitations," International Journal of Non-Linear Mechanics, vol. 25, (5), pp. 455–474, 1990.

Vita

Khalid Bassam Adnan Idries Al-Souqi was born in 2000, in Dubai, United Arab Emirates. He received his primary and secondary education in Sharjah. UAE. In 2022, he received his B.Sc. degree in Mechanical Engineering from the University of Sharjah. In January 2023, he joined the Mechanical Engineering master's program at the American University of Sharjah as a graduate research assistant. His research interests are in vibration-damping systems and nonlinear dynamics.